JCI The Journal of Clinical Investigation

# CDKL3 is a targetable regulator of cell cycle progression in cancers

Haijiao Zhang, … , Shixue Wang, Ren Sheng

*J Clin Invest.* 2024. https://doi.org/10.1172/JCI178428.

Research In-Press Preview Cell biology Therapeutics

## Graphical abstract

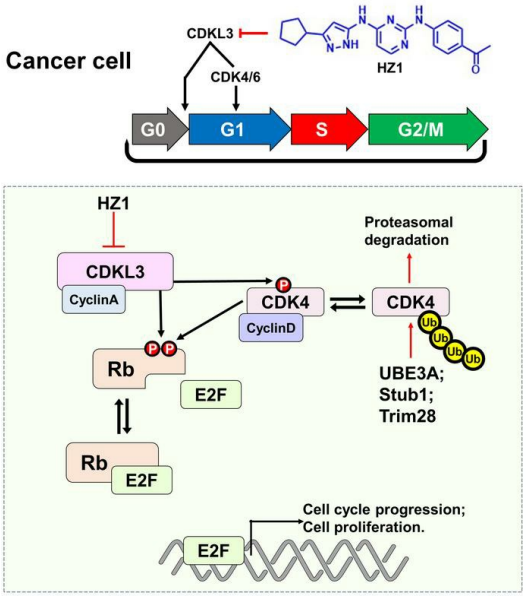


## Find the latest version:

https://jci.me/178428/pdf

**Title page**

# CDKL3 is a targetable regulator of cell cycle progression in cancers

Haijiao Zhang[1,#], Jiahui Lin[1,#], Shaoqin Zheng[1], Lanjing Ma[1], Zhongqiu Pang[1], Hongyi Yin[1], Chengcheng Meng[2], Yinuo Wang[1], Qing Han[1], Xi Zhang[3], Zexu Li[1], Liu Cao[4], Lijun Liu[1], Teng Fei[1], Daming Gao[5], Liang Yang[6], Xueqiang Peng[6], Chen Ding[1,*], Shixue Wang[7,*], Ren Sheng[1,8,*]

[1]College of Life and Health Sciences, Northeastern University, Shenyang 110819, China.

[2]Department of Pathology, the Fourth People's Hospital of Shenyang, Shenyang 110083, China

[3]College of Sciences, Northeastern University, Shenyang 110004, China.

[4]College of Basic Medical Science, China Medical University, Shenyang 110122, China.

[5]State Key Laboratory of Cell Biology, CAS Center for Excellence in Molecular Cell Science, Shanghai Institute of Biochemistry and Cell Biology, Chinese Academy of Sciences, Shanghai 200031, China.

[6]Department of General Surgery, the Fourth Affiliated Hospital, China Medical University, Shenyang 110032, China.

[7]State Key Laboratory of Electroanalytical Chemistry, Changchun Institute of Applied

Chemistry, Chinese Academy of Sciences, Changchun 130022, China

[8]Lead contact

#These authors share equal contribution

*Correspondence:

Ren Sheng (R.S.):

Email: shengren@mail.neu.edu.cn; TEL: +86-13944806789; Mailing address: 195 Chuangxin Road, Hunnan District, Shenyang, Liaoning, China, 110819.

Shixue Wang (S.W.):

Email: wangsx@ciac.ac.cn; TEL: +86-13756116863; Mailing address: 5625 Renmin Street, Chaoyang District, Changchun, Jilin, China, 130022.

Chen Ding (C.D.):

Email: dingchen@mail.neu.edu.cn; TEL: +86-13644079688; Mailing address: 195 Chuangxin Road, Hunnan District, Shenyang, Liaoning, China, 110819.

**Conflict of Interest**

We declare the following financial interests/personal relationships which may be considered as potential competing interests: A patent has been filed by R.S. and S.W. related to this work (Patent application NO. 2023115696895).

**Abstract**

Cell cycle regulation is largely abnormal in cancers. Molecular understanding and therapeutic targeting of the aberrant cell cycle are essentially meaningful. Here, we identified an under-appreciated Serine/Threonine kinase, CDKL3 (Cyclin-Dependent Kinase Like 3), crucially drives the rapid cell cycle progression and cell growth in cancers. Mechanism-wise, CDKL3 localizes in the nucleus and associates with specific cyclin to directly phosphorylate Retinoblastoma (Rb) for quiescence exit. In parallel, CDKL3 prevents the ubiquitin-proteasomal degradation of CDK4 by direct phosphorylation on T172 to sustain G1 phase advancement. The crucial function of CDKL3 in cancers was demonstrated both in vitro and in vivo. We also designed, synthesized and characterized a first-in-class CDKL3-specific inhibitor, HZ1. HZ1 exhibits greater potency than CDK4/6 (Cyclin-Dependent Kinase 4/6) inhibitor in pan-cancer treatment by causing cell cycle arrest and overcomes the acquired resistance of the latter. In particular, CDKL3 has significant clinical relevance in colon cancer, and the effectiveness of HZ1 was demonstrated by murine and patient-derived cancer models. Collectively, this work presented an integrated paradigm of cancer cell cycle regulation and suggested CDKL3-targeting as a feasible approach in cancer treatment.

## Maintext

## Introduction

The cell cycle consists of multiple modules and machineries to regulate the cell division in a precise manner (1, 2). A complete cell cycle is composed of G1, S, G2 and M phases sequentially. The progression of cell cycle is primarily governed by cyclins and Cyclin-Dependent Kinases (CDKs) at various stages (2, 3). For instance, the pair of CDK4/6-cyclin D is known to maintain the G1 phase forwarding (4). At the G1/S phase checkpoint, the combination of CDK1/2-cyclin E/A takes over the responsibility for G1-to-S transition (4, 5). In both processes, the phosphorylation of Rb protein by CDKs is essentially required (3, 4). The phosphorylated Rb (i.e., on S807/S811) can dissociate with the transcription factor E2F, leading to the expression of multiple cell cycle related genes which are required in the ensuing phases (6).

Besides the active cycling, cells can exit the cell cycle and stay in a resting/quiescent state called G0 phase. Cells in this state are generally found non-dividing and non-growing (7). The regulation of G0 entry and exit remains obscure. An earlier literature suggested CDK3-cyclin C to support the G0-to-G1 transition by phosphorylation of Rb (8). However, CDK3 in most laboratory mice harbors the natural loss-of-function mutation with no phenotypic defects (2, 4). Hence, the biological importance of CDK3 in G0 phase exit was undermined by this phenomenon. Despite that new factors have been reported to regulate this transition in recent years (9, 10), the understanding of this process is still largely lacking (7).

Cell cycle is often dysregulated in cancer (2, 7). Normal cells have clear schedule on their cell cycle entry and exit. However, various types of (epi)genetic changes allow the cancer cells to bypass the resting phase (7). Thereby, in cancers, the accelerated and uncontrolled cell cycle is widely seen, which is favored for the infinite mitogenic proliferation (7). Targeting cell cycle progression has been shown effective in cancer therapy (11, 12). Due to the central role in cell cycle regulation and the enzymatic nature of CDKs, multiple small molecule inhibitors against CDKs are designed and tested in clinical trials or have been clinically approved in cancer treatment (11, 12). However, clinical feedbacks pointed out the challenge of the acquired drug resistance of these inhibitors (13). The discovery of new targets to overcome it is hence of greater need and value.

CDKL3 belongs to Cyclin-Dependent Kinase Like (CDKL) kinase subfamily, which is part of CMGC Ser/Thr protein kinase superfamily. CDKL kinases share the conserved α-helix on the kinase domain of CDK as the putative cyclin-binding site (14-16). However, whether CDKL could bind cyclins or function via cyclins is unknown. In fact, CDKL family is overall underexplored in terms of both function and mechanism. CDKL5 has been shown related to neurological disorders, whereas CDKL1 was reported to regulate cilia formation (17-19). Despite CDKL3 was reported to associate with cancer progression (20-22), the mechanism requires further scrutiny with rigorous evidence.

Here, we report that CDKL3 directly promotes cell cycle progression in cancer. Two parallel regulatory paths exist molecularly. First, CDKL3 couples with cyclin A2 to directly lead to Rb phosphorylation and G0-to-G1 transition. Ablation of CDKL3 results in the cell cycle exit and growth retardation in cancers. Also, CDKL3 can phosphorylate CDK4 on T172 with the assistance of cyclin A2. This leads to the consequence that CDK4 avoids undergoing ubiquitin-proteasomal dependent degradation, thereby sustaining G1 phase progression. E3 ubiquitin ligases such as Trim28 cause CDK4 ubiquitination in the absence of T172 phosphorylation. Moreover, we rationally designed and characterized small-molecule inhibitor HZ1 specifically against CDKL3. HZ1 showed strong tumor-suppressing effect with $IC_{50}$ at nanomolar range and the potential to overcome the resistance of CDK4/6 inhibitor, and manifested satisfactory tumor clearance on laboratory animals and patient-derived samples. Together, we have discovered a series of mechanistic findings on the critical role of CDKL3 in cell cycle regulation and revealed the cyclin-dependent function of CDKL subfamily kinase. Besides the value in basic biomedical research, this work also presented and proposed an alternative cancer therapeutic approach by targeting CDKL3-mediated cancer cell cycle progression.

## Results

### CDKL3-loss abrogates cancer cell growth by impeding G0-to-G1 transition

Similar to CDK family kinases, CDKL kinases contain the conserved putative cyclin

binding α-helix (14-16, 19) (Figure 1A). CDKL3 also has a potential nucleus-localization sequence (NLS) by prediction that is conserved among different species (Supplemental Figure 1A). We speculated that CDKL3 might be ready to localize in the nucleus and regulate cell cycle in a manner reminiscent of CDKs. CDKL3's subcellular location was inspected to test this assumption. Immunofluorescence has demonstrated that endogenous CDKL3 localizes largely in the nucleus with a small amount in the cytoplasm (Figure 1B and Supplemental Figure 1, B and C). And this nuclear localization was largely cell cycle phase-independent (Supplemental Figure 1D). We found that CDKL3 could no longer effectively dwell in the nucleus after internal deletion of the putative NLS (Figure 1C). After the insertion of the NLS of CDKL3, tandem GFPs (Green Fluorescent Proteins), which could only stay in the cytosol, became able to translocate into the nucleus (Figure 1C).

Next, we sought to determine whether CDKL3 affected the cell cycle progression. CRISPR-Cas9 system was employed to generate multiple CDKL3 knockout (KO) cancer cell lines (Supplemental Figure 1, E-G). According to the flow cytometry experiment of BrdU/Propidium Iodide (PI) dual-staining, KO of CDKL3 significantly raised the fraction of G0/G1 phase while significantly decreasing the percentage of S phase under both normal and serum starvation conditions (Figure 1, D-F and Supplemental Figure 1, H-K). The recovery of CDKL3 effectively reversed the situation (Figure 1, D-F). Immunofluorescent intensity of BrdU incorporation per cell and the number of BrdU-positive cells supported the stalled G0/G1-to-S transition

(Figure 1, G-I and Supplemental Figure 1, L-O) (23).

We then had a closer look at G0/G1 phase. By serum starvation, the cells can be synchronized to G0 phase, the release of which was able to reveal the process of cell cycle re-entry from quiescence (24). In this assay, we visualized that upon CDKL3 KO the appearance of phosphorylated Rb (pRb) and cyclin D1 were substantially delayed and diminished (Figure 2A and Supplemental Figure 1, P-R). Even after release for thirty hours, both pRb and cyclin D1 showed minimal levels when CDKL3 was ablated (Figure 2A and Supplemental Figure 1, P-R). These two served as strong markers of cell cycle progression from G0/G1 towards S phase (2, 3). Later, we further discriminated G0 and G1 phases by Pyronin Y/PI staining (8, 10). The flow cytometry result showed that in multiple cell lines CDKL3 ablation markedly caused an increased proportion of G0-phased cells with strong statistical significance (Figure 2, B-D and Supplemental Figure 1, S-V). The protein and transcription levels of several G0 phase markers also increased after CDKL3 ablation, which supported the flow cytometry data (Figure 2, E and F and Supplemental Figure 1, W-Z) (25, 26). Moreover, depletion of CDKL3 resulted in evident growth defects in these cancer cell lines, which was in accordance with the cell cycle arrest (Figure 2G and Supplemental Figure 1, AA and AB). Further evidence to support that CDKL3 positively regulated cancer cell growth was provided by the three-dimensional colony formation (Figure 2, H and I and Supplemental Figure 1, AC-AE). Together, we demonstrate CDKL3 promotes the cell cycle and cell growth in multiple cancer cells.

CDKL3-loss leads to the severe delay of G0-to-G1 and G1-to-S transitions and thus prevents cancer cell cycle progression.

**CDKL3 phosphorylates Rb for cell cycle entry when coupling with cyclin A2**

We further interrogated the mechanism of cell cycle regulation by CDKL3. As CDKL3 was positively correlated with pRb level, we hypothesized Rb as a direct substrate of CDKL3 (Figure 2A and Supplemental Figure 1, Q and R). Due to the presence of the conserved α-helix on the kinase domain, we first questioned whether CDKL3 could interact with any cyclin before further investigation. We observed that several cyclins, including A2, B1, D1, and E1, bound CDKL3 both exogenously and endogenously through co-immunoprecipitation (co-IP) (Figure 3, A and B and Supplemental Figure 2A). The binding between CDKL3 and cyclin A2 remained unchanged at different cell cycle phases, as the binding of other cyclins to CDKL3 moderately fluctuated (Supplemental Figure 2B). When the conserved α-helix was truncated, the binding was greatly impaired (Figure 3C). However, the point mutation of RXL motif, another motif suggested to be involved in cyclin binding (27, 28), showed minimal difference from wild-type (WT) CDKL3 for the binding (Figure 3C). In addition, we demonstrated that endogenous CDKL3 can bind to Rb (Figure 3B). The mapping study pointed out that the carboxyl-terminal of CDKL3, which also contained the NLS motif, was primarily involved in Rb binding (Figure 3, D and E). CDK inhibitors such as p21, p27 and p16 were shown incapable of interacting CDKL3 (Supplemental Figure 2C) (2).

To determine whether Rb was the direct substrate of CDKL3, we exercised in vitro kinase assay. Two truncations (a.a. 379-928 and 792-928) containing the phosphorylation sites (S807/S811) were widely accepted in vitro because the size of full-length Rb was too large for bacterial expression (6, 29, 30) (Figure 3F). We constructed both truncations and purified the expressed protein from *E.coli*. In the absence of cyclin, it was evident that CDKL3 was unable to phosphorylate Rb (Figure 3G). Introduction of cyclin A2 and E1 into the reaction system could lead to substantial phosphorylation of Rb on S807/S811 by CDKL3, whereas B1 and D1 behaved otherwise (Figure 3G and Supplemental Figure 2D). The CDKL3-cyclin A2 pair was comparable to the traditional CDK4/6-cyclin D1 coupling in Rb phosphorylation strength in vitro (Figure 3H and Supplemental Figure 2E).

We intended to evaluate the functionality of a kinase-dead mutant to confirm the contribution of CDKL3's kinase activity to Rb phosphorylation. However, the activation site of CDKL3 was unidentified and the loss-of-function mutant thus remained to be determined. We made a number of point mutations on the putative ATP binding site (K33), the conserved aspartic acid (D125) and the MAPK (mitogen-activated protein kinase)-mimicking activation loop (T158/Y160) of CDKL3 (Supplemental Figure 2F). Via in vitro kinase assay, it was discovered that K33E and D125K both led to the loss of CDKL3 kinase activity (Figure 3I). Meanwhile, the conserved α-helix truncation mutant (Δα), which lost cyclin binding capacity, was unable to phosphorylate Rb in vitro in the presence of cyclin (Figure 3J). Neither did

the combinatory mutant of K33E/D125K or Δα promote Rb phosphorylation nor restore the cell cycle progression in CDKL3 KO cells (Supplemental Figure 2G). We next determined whether both cyclin A2 and E1 could co-operate with CDKL3 for cell cycle regulation in cell. In U2OS cell where CDKL3 was ectopically expressed, phosphorylation of Rb was apparently accelerated after serum starvation and release (Figure 3K). This effect, however, could only be neutralized by the depletion of cyclin A2 instead of E1 (Figure 3K and Supplemental Figure 2, H-K). And only when cyclin A2 was depleted did BrdU incorporation, a clear indication of cell cycle progression into S phase, become impaired (Figure 3, L and M) (23). Since CDK2 also requires cyclin A2 to function at G1/S checkpoint, we further interrogated the relationship between CDKL3 and CDK2. The in vitro competition assay revealed that cyclin A2 has higher affinity toward CDKL3 than CDK2 (Supplemental Figure 2, L and M). Since the amount of cyclin A2 is low at cell quiescence, we hypothesize that cyclin A2 preferably interacts with CDKL3 for cell cycle entry. When cyclin A2 gradually becomes abundant along with the progression of cell cycle, CDK2 then will receive sufficient cyclin A2 for activation, hence functioning as the critical factor in G1-to-S transition (Supplemental Figure 2N).

Together, these results indicate that CDKL3 serves as the kinase that can directly phosphorylate Rb on the conventional S807/S811 sites. In this event, CDKL3 uses the conserved putative cyclin-binding α-helix in its kinase domain to interact with cyclins, in particular cyclin A2, to enable the phosphorylation of Rb for cell cycle

initiation. The fruit of this event can be further handed into the classical CDK-cyclin pairs to sustain the hyper-phosphorylation of Rb and eventually overcome the G1/S phase checkpoint.

**CDKL3 phosphorylates CDK4 on T172 to promote CDK4 stability via K48-linked poly-ubiquitination prevention**

We found an unexpected but intriguing behavior when we monitored pRb. In all CDKL3 KO cell lines, CDKL3 ablation remarkably reduced the endogenous CDK4 protein levels (Figure 4A). After multiple attempts, we realized the pattern was highly reproducible. To investigate it, we first checked the transcription of CDK4. The RT-qPCR results showed that CDKL3 ablation did not affect CDK4 transcriptionally (Supplemental Figure 3A). Alternatively, the cycloheximide (CHX)-blocking experiment was used to determine the protein stability of CDK4. It appeared that CDK4 protein stability and CDKL3 had a strong positive correlation, supporting our finding in Figure 4A (Figure 4B and Supplemental Figure 3B). Further demonstration of protein ubiquitination revealed that the presence of CDKL3 markedly reduced the poly-ubiquitination of CDK4 (Figure 4C). The particular change of poly-ubiquitination on CDK4 was K48-linked (Figure 4C), which agreed with the well-known biological function of K48-linked poly-ubiquitination in protein degradation (31).

We used the in vitro kinase assay to determine if CDK4 was the direct substrate of CDKL3. According to previous researches, CDK7 was able to phosphorylate CDK4

on a conserved threonine, T172 (32, 33). This event was reported to promote CDK4 activity and vitally control cell cycle. We therefore interrogated whether CDKL3 could phosphorylate the same site. Enlightened by our earlier finding, we tested the four cyclins that could bind CDKL3 by in vitro kinase assay and used CDK7 as the stringent control. The data showed that cyclin A2 and D1 could both assist WT CDKL3 to directly phosphorylate CDK4 on T172 (the kinase-inactive CDK4 was used as the substrate to avoid self-phosphorylation) (34), while the kinase-dead mutant K33E/D125K of CDKL3 failed to accomplish so (Figure 4, D and E). Co-IP assays also showed that the carboxyl region of CDKL3 interacted with CDK4, fulfilling the requirement of potential kinase-substrate relationship (Figure 3B and 4F). These observations were further consolidated by the data that the kinase-dead mutant of CDKL3 behaved deficient to phosphorylate CDK4 or to reduce CDK4 ubiquitination endogenously (Figure 4G and Supplemental Figure 3C).

According to these clues, we proposed that phosphorylation on T172 of CDK4 could promote its protein stability by avoidance of ubiquitination. By the KO-and-rescue approach, we observed that the phosphorylation-gain mimicking mutant T172E showed minimal ubiquitination, whereas the phosphorylation-loss mimicking mutant T172A was highly poly-ubiquitinated (Figure 5A and Supplemental Figure 3D). Treatment of proteasome inhibitor MG132 could substantially stabilize T172A to the same extent of WT and T172E, which confirmed the involvement of proteasomal degradation pathway (Figure 5B and Supplemental Figure 3D). From the CHX-

blocking assay, it was seen that T172E was markedly stabler than CDK4 WT, whereas T172A only maintained a basal protein level, indicating its low protein stability (Figure 5C and Supplemental Figure 3, E-G). T172E in CDKL3 KO cells appeared as stable as WT CDK4 in CDKL3-rescued cells (Figure 5D and Supplemental Figure 3H). T172A, on the other hand, showed imminent protein degradation either in the presence or absence of CDKL3 (Figure 5D and Supplemental Figure 3H). In CDK4 KO cells, rescue of T172A failed to recover G1 progression as shown by both immunoblotting and flow cytometry, which further illustrated the functional importance of the phosphorylation (Figure 5, E and F and Supplemental Figure 3I). Regarding the functional relevance of cyclins in the cellular context, depletion of cyclin A2 was incapable of stabilizing CDK4 even in the presence of surplus CDKL3 (Figure 5G and Supplemental Figure 3J). Since the depletion of cyclin D1 was reported to cause the strong compensation by cyclin D2 and D3 (35-37), the loss of function study of D1 was involuted due to the technical limitation. We therefore knocked down all three to confirm the involvement of cyclin D (Supplemental Figure 3K). The CHX-blocking data revealed that depletion of cyclin D did not affect the stability of CDK4 either with endogenous or ectopically expressed CDKL3 (Figure 5H and Supplemental Figure 3L).

Combining the findings on the phosphorylation of Rb and CDK4 by CDKL3, we tested the regulatory role of CDKL3 in cancer cell proliferation in vivo. On the nude mice, we transplanted the parental, CDKL3 KO, and CDKL3 overexpressed (OE)

303 strains of DLD-1 cells. It was convincingly proved that transplanted CDKL3 KO DLD-
304 1 cells hardly developed into tumors (Figure 5, I and J and Supplemental Figure 3M).
305 Overexpression of CDKL3, on the other hand, considerably enlarged the tumors in
306 vivo when compared with the parental group (Figure 5, I and J and Supplemental
307 Figure 3M). As expected, this effect can be effectively neutralized by the knockout of
308 CDK4 (Supplemental Figure 3, N-P). In the transplanted tumors, we also observed
309 that pRb and CDK4 were markedly reduced when CDKL3 was depleted by both
310 immunohistochemistry (IHC) and immunoblotting (Figure 5K and Supplemental
311 Figure 3Q). Conversely, pRb and CDK4 levels were further elevated under CDKL3
312 overexpression condition (Figure 5K and Supplemental Figure 3Q). This data
313 demonstrated that CDKL3 caused cancer cell proliferation by promoting cell cycle
314 progression in vivo, which concurred with the in vitro conclusions. Taken together, we
315 found that CDKL3 directly phosphorylates T172 on CDK4. This process requires
316 cyclin A2 and prevents the ubiquitin-proteasomal degradation of CDK4. Consequently,
317 CDKL3 can assist the cell cycle progression and cell proliferation in cancer via “dual
318 paths” - CDK4 stabilization and Rb phosphorylation in parallel. CDKL3 therefore can
319 both trigger G0-to-G1 transition and sustain G1 progression.
320
321 **Trim28 ubiquitinates CDK4 for protein degradation in the absence of T172**
322 **phosphorylation**
323 We next set out for the specific protein that senses CDK4 phosphorylation and
324 governs CDK4 ubiquitination. Stub1 and UBE3A, two E3 ubiquitin ligases, have been

linked to CDK4 ubiquitination in prior researches (38, 39). We verified that CDK4 WT and T172A can be ubiquitinated by both ligases, with T172A exhibiting higher poly-ubiquitination level than WT CDK4 (Figure 6A). When T172 was mutated to glutamic acid, neither could Stub1 nor UBE3A be operative (Figure 6A). From Mass-spec database on protein-protein interaction (40), we also identified a nuclear-localized and CDK4-binding E3 ligase, Trim28 (41), to be capable of CDK4 ubiquitination (Figure 6A). Like Stub1 and UBE3A, Trim28 failed to ubiquitinate CDK4 T172E while being active on CDK4 WT and T172A (Figure 6A). The co-IP assay showed that T172E had poorer binding capacity with all three E3 ligases (Figure 6B), suggesting that the phosphorylation of T172 might be unfavored by these E3 ligases in terms of the substrate recognition.

Trim28 was further characterized. Depletion of Trim28 attenuated the overall poly-ubiquitination of CDK4 (Figure 6, C and D and Supplemental Figure 4, A-D). Additionally, Trim28 enzymatic-dead mutant (42) (C65A/C68A) failed to ubiquitinate CDK4, supporting the requirement for the ligase activity (Figure 6E). The direct enzyme-substrate relationship between Trim28 and CDK4 was further validated by in vitro ubiquitination assay, in which CDK4 was purified from bacteria with zero basal ubiquitination background (Figure 6F). Endogenously, Trim28 depletion reduced CDK4 ubiquitination and increased CDK4 protein stability, whereas overexpressed Trim28 further diminished CDK4 stability (Figure 6G and Supplemental Figure 4E). Function-wise, perturbation of Trim28 (overexpression or depletion), however, did not

affect cancer cell growth or cell cycle (Supplemental Figure 4, F-H). We hypothesized that this was due to the redundancy or compensation of CDK6 or other E3 ligases. Also, by literature search, we realized that Trim28 had several cell cycle related proteins as substrates (such as Rb and cyclin A2) (41, 43, 44). Thus, Trim28 could exert complicated influence on cell cycle, which is likely context-dependent. Nevertheless, this mystery does not affect the claim of CDK4 being a direct substrate of Trim28. CDK4 ubiquitination (and ensuing degradation) is sensitive to the phosphorylation on T172, but unspecific to a particular E3 ubiquitin ligase.

**CDK inhibitors do not affect CDKL3 kinase activity**

We next sought to find the small molecule to block CDKL3 in order for cell cycle arrest. To date, CDK4/6 inhibitors and CDK1/2 inhibitors are widely used in clinical therapies or under clinical trials due to their pan-cancer killing effects (Figure 7A) (11, 12). We thus tested the possible inhibitory effect of these inhibitors on CDKL3. From the in vitro kinase assay, we observed that CDK2 inhibitor (45) (Cdk1/2 Inhibitor III) could effectively inhibit CDK2 but exerted no effect on CDKL3 when phosphorylating Rb (Figure 7B). Since CDK1/2 primarily governs the entry of S phase from G1, we used double thymidine blocking to synchronize cells right at the G1/S checkpoint to explore this process (46). The results supported our earlier discovery that CDKL3 primarily functioned in G0-to-G1 transition and G1 phase. CDKL3 ablation or overexpression had minimal impact on S phase entry of the cancer cells (Figure 7C and Supplemental Figure 5, A-C). In all circumstances, the treatment of CDK2

inhibitor led to the complete disappearance of pRb and cyclin D1 (Figure 7C and Supplemental Figure 5, A-C). This data validates that CDKL3 cannot replace the function of CDK1/2 at G1-to-S transition.

Meanwhile, we tested CDK4/6 inhibitor (47) in vitro. The data demonstrated that the CDK4/6 inhibitor Palbociclib could only effectively target CDK4 rather than CDKL3 for inhibition (Figure 7D). To observe G0-to-G1 transition and the progression of G1 phase, serum starvation was employed to synchronize cells at G0. In the cancer cells, the accumulation of pRb halted when CDKL3 was ablated and accelerated with ectopic CDKL3 (Figure 7E and Supplemental Figure 5, D-F). However, in all conditions, treatment with CDK4/6 inhibitor resulted in the elimination of pRb and cyclin A2 (Figure 7E and Supplemental Figure 5, D-F). This came as a surprise because, according to our hypothesis, CDKL3 functions prior to CDK4/6; as a result, Rb phosphorylation by CDKL3 should appear shortly after serum release in the presence of CDK4/6 inhibitor but unlikely further augment in an extended period. From literature reading and the data analysis, we also noticed a well-documented side-effect that cyclin A2 can be ameliorated by CDK4/6 inhibitor treatment (48, 49). It was very likely that CDK4/6 inhibition disabled E2F for *CCNA2* (gene name of cyclin A2) expression. Though the kinase activity of CDKL3 was not affected by Palbociclib, it required cyclin A2 to function (Figure 3K). Thus, why Rb remained unphosphorylated could be explained (Figure 7E and Supplemental Figure 5, D-F). When we ectopically expressed cyclin A2, CDKL3 indeed could partially sustain Rb

391 phosphorylation and G1 progression (Figure 7F). But CDKL3 could hardly
392 compensate the function of CDK4/6 in sustaining substantial Rb phosphorylation
393 required for cell cycle advancement in full.
394
395 Together, these results suggest that neither CDK1/2 nor CDK4/6 inhibitor affects
396 CDKL3 kinase activity. CDKL3 cannot replace the function of CDK1/2 in G1/S
397 transition or that of CDK4/6 in maintaining adequate Rb phosphorylation in G1. The
398 design and characterization of a first-in-class CDKL3 inhibitor is necessary, which
399 can potentially provide an alternative therapeutic path in cancer treatment by causing
400 cell cycle arrest.
401
402 **Design and characterization of CDKL3 inhibitor**
403 According to the previous publication, a potential CDKL3 inhibitor candidate caught
404 our attention. From a chemical screening study, it was discovered that a compound
405 named ASC67 could bind to the catalytic pocket of CDKL3 kinase domain with
406 satisfactory selectivity over other related kinases, yet the functional demonstration
407 was absent (Figure 8A) (19). Following that, we intended to generate an efficient
408 CDKL3 inhibitor based on this chemical backbone in order for cell cycle arrest. As the
409 first step, the original compound (ASC67) was synthesized and the performance was
410 evaluated (50). The addition of ASC67 could gradient-dependently diminish the
411 phosphorylation of Rb by CDKL3 while remaining uninfluential to CDK4 or CDK2 in
412 vitro (Figure 8B). The effectiveness of this chemical was then evaluated using a

variety of cancer cell lines including the estrogen-responsive (ER+) breast cancer where Palbociclib (Palbo) is administrated clinically (51). All cell lines that were treated with ASC67 for 24 and 72 hours shown significant tumor-suppressing effects, with $IC_{50}$ values with the median of 500 nanomolar (Figure 8, C-F and Supplemental Figure 6, A-F). As a direct comparison, the clinically approved CDK4/6 inhibitor had the $IC_{50}$ value ranging from 1 to 5μM in different cell lines (Figure 8, C-F and Supplemental Figure 6, A-F) (47, 52-55). This information made it evident that ASC67 holds considerable promise in cancer treatment and can be used as a backbone compound for further optimization.

We further conducted rational design to enhance the affinity and effectiveness of CDKL3 inhibitor based on ASC67. From the structural analysis, we realized the central pyrimidine group of ASC67 forms multiple key hydrogen bonds with CDKL3, which was not recommended to be replaced (Figure 8A). And the cyclopentane group forms π-π interaction with the side chain of Phe80 to stabilize the hydrophobic pocket residence (Figure 8A). We hence focused on the cyan group of this molecule and proposed several polar functional groups for substitution (Figure 8G). All molecules were produced by organic synthesis. After tests, a few replacements showed lessened CDKL3 inhibitory impact. Fortunately, C3I-22, one of the compounds, had a much lower $IC_{50}$ value for clearing cancer cells compared to the backbone molecule (Figure 8, H-J). From the numbers, we could see C3I-22 had increased the effectiveness for 3-4 folds compared to ASC67 (Figure 8, H-J and

Supplemental Figure 6, A and D). Consistently, C3I-22 also showed a lower threshold for substrate phosphorylation in vitro (Figure 8K). Biophysical detection (by Surface Plasmon Resonance assay) clearly indicated that the binding affinity between CDKL3 and C3I-22 was 5-fold higher than that between CDKL3 and ASC67 (Figure 8, L and M and Supplemental Figure 6, G and H). To test the cellular selectivity of the ASC67 derivatives, we designed and synthesized the orthogonal PEG (polyethylene glycol)-linked biotinylated derivatives (C3I-PEG3-Biotin) for cellular content pull-down assay by streptavidin resins (Supplemental Figure 6I). After treatment to the cells, the protein bound to C3I-PEG3-Biotin was harvested after cell lysis and dialysis. It showed that cellular CDKL3 could be effectively captured by C3I-PEG3-Biotin instead of CDK2 and CDK4/6 (Figure 8N). Hence, we argue that the selectivity of ASC67 derivatives is adequate. We further genetically modulated CDKL3, CDK4 and Rb in the cells to examine whether C3I-22 restrained cell cycle specifically through CDKL3-mediated events. As expected, cells with ectopic expression of CDKL3 and CDK4 both required greater amount of C3I-22 to suppress cell growth; knockout of CDK4 or increased amount of Rb led to reduced $IC_{50}$ value; depletion of CDKL3 or Rb made the cells insensitive to C3I-22 treatment (Table 1 and Supplemental Figure 1, E and F and Supplemental Figure 3E and Supplemental Figure 6, J-S). These results thus further confirmed the specificity of C3I-22 and our mechanistic model. Together, we demonstrated the feasibility of CDKL3 inhibitors and the improved potency of C3I-22 with satisfactory specificity.

**C3I-22 (HZ1) antagonizes cancer growth via cell cycle arrest in multiple models**

Besides the cell growth suppression effect, we further examined C3I-22 molecularly. Under the cellular context, C3I-22 treatment reduced the levels of pRb and CDK4 (Figure 9A and Supplemental Figure 7A), and caused the failure of rapid cell cycle progression in cancer cells shown by flow cytometry (Figure 9, B and C and Supplemental Figure 7, B and C). Besides, the treatment of C3I-22 could overcome the acquired drug resistance of CDK4/6 inhibitor in ER+ breast cancer (Table 2 and Supplemental Figure 7D). The cell cycle of the resistant cell lines showed high sensitivity to C3I-22 treatment, thus further promising the therapeutic value of C3I-22 (Figure 9, D and E and Supplemental Figure 7, E and F). Further interrogation revealed that not only could C3I-22 remove the existing resistance of CDK4/6 inhibitor but also sensitize the cells to CDK4/6 inhibitor (Figure 9, F-I) (56). We reason that C3I-22 could act on a different stage (G0-to-G1 transition) from CDK4/6 inhibitor and meanwhile suppress the elevated CDK4/6 protein level, which was often the cause of acquired resistance (13, 57). On a different note, improved potency was not seen in the compounds which was further developed based on C3I-22 (Supplemental Figure 7, G and H). Thus, we focused on C3I-22 for functional tests in this study.

We examined C3I-22's ability to inhibit tumors in vivo. We first tested the therapeutic effect of C3I-22 in the xenograft model. Administration of a very low dosage of C3I-22 could already effectively clear the tumor burden of the transplanted DLD-1 cells and

mitigate the levels of pRb and CDK4, and within the period of treatment the mice displayed no severe liver and kidney toxicity (Figure 9, J-L and Supplemental Figure 7, I-K). Another mouse model was also employed to demonstrate the efficacy of this inhibitor. In *Apc*$^{min/+}$ mice, a well-documented model which forms spontaneous colorectal cancer (58, 59), treatment of C3I-22 significantly reduced the tumor number and volume (Figure 9, M and N and Supplemental Figure 7, L and M). Histological data also showed that the intestinal architecture restored and the proliferation marker Ki67 diminished after treatment (Supplemental Figure 7N). Thus, we eventually renamed C3I-22 as HZ1 for further characterization. Together, we have rationally designed and developed a first-in-class CDKL3 inhibitor HZ1. HZ1 showed substantial promise as a therapy for cancer since it effectively blocks CDKL3-mediated cell cycle progression both in vitro and in vivo.

**HZ1 has strong clinical implication in colon cancer treatment**

We analyzed multiple cancer clinical database to further demonstrate the potential clinical importance of CDKL3. The transcriptome databases showed that CDKL3 expressed much higher in the colon cancer tissue than the normal adjacent tissues (Figure 10A) (60). This was confirmed by immunohistochemical images of the colon cancer patients (Figure 10, B and C and Supplemental Table 1). Significant difference between cancer and normal tissues was also seen for CDK4 and pRb (Supplemental Figure 8, A-D). Both CDK4 and pRb positively correlates with CDKL3 in the colon cancer tissues (Supplemental Figure 8, E and F). Additionally, a strong

correlation existed between the high level of CDKL3 and poor prognosis for colon cancer patients (Figure 10D) (61). All these clues together suggested CDKL3 was unfavored in colon cancer.

The patient-derived organoid is widely acknowledged and welcomed for both fundamental and translational cancer research due to the strong clinical relevance (62). We collected the primary colon cancer samples from the patients and cultured them according to the protocols (62). After seven days of culturing, two out of three samples successfully formed structured organoids which could be stably maintained (Supplemental Figure 8G). We first depleted CDKL3 in the organoids to observe the effects (Supplemental Figure 8, H and I). After CDKL3 depletion, the organoids dissociated and failed to survive (Figure 10, E and F). Immunoblotting verified that both CDK4 and pRb levels clearly dwindled (Figure 10G). Afterwards, we tested the potency of HZ1 on these samples. With the increased administered doses, the colon cancer organoids clearly showed a rising proportion of dissociation and death (Figure 10, H-J and Supplemental Figure 8, J-L). Treatment of HZ1 could eradicate almost 100% of the patient tumor organoids with 72 hours at the concentration of 5μM (Figure 10, H-J and Supplemental Figure 8, J-L). The proliferation marker Ki67 vanished after 24 hours of HZ1 treatment as shown by immunofluorescence (Figure 10K). Under 1μM HZ1 administration for 5 days, 80-90% colon cancer organoids died (Figure 10, L and M and Supplemental Figure 8, M and N). Similar to the data obtained from cell lines, HZ1 markedly decreased the levels of pRb and CDK4

(Figure 10N and Supplemental Figure 8O), hence effectively triggering cell cycle arrest and tumor death. We also interrogated the response of the cancer organoids to HZ1 with the genetical modulations of CDKL3, CDK4 or Rb. Consistent with the cell line data, cancer organoid became more sensitive to HZ1 with the depletion of CDK4 or increased expression of Rb (Figure 10, O and P and Supplemental Figure 8, P-V). Forced expression of CDKL3 and CDK4 both required higher HZ1 concentration to inhibit organoid growth (Figure 10O and Supplemental Figure 8, R-U). And organoids with CDKL3 or Rb depletion were insensitive to the treatment (Figure 10P and Supplemental Figure 8, P-T and V). Collectively, we have established a robust clinical connection between CDKL3 and colon cancer overall. CDKL3 inhibitor such as HZ1 could efficiently clear the tumor burden derived from the colon cancer patient. These results strongly implicate that HZ1 and CDKL3-targeting strategy has great translational potential in clinic.

## Discussion

In this work, we identified CDKL3 as a crucial regulator of cell cycle progression in cancer, by phosphorylation of Rb to initiate cell cycle from quiescence and preserving CDK4 to maintain G1 phase advancement. These two events both contribute to the accelerated cell cycle that is required for rapid growth in cancers. The proposed small molecule inhibitor against CDKL3 was shown for its great potency in cancer treatment. We discovered that CDKL3 may function in pair with cyclin A2 at the G0-to-G1 transition. Unlike cyclin D, cyclin A2 is present in G0 phase, which is readily

545 engaged by CDKL3. Therefore, CDKL3-cyclin A2 together run the first leg in the
546 “relay race” of cell cycle. CDKL3-loss caused severely delayed G0-to-G1 transition
547 and alleviated cancer cell growth.
548
549 Meanwhile, CDKL3 can give a big push to the “second leg runner” CDK4. Through
550 direct phosphorylation on CDK4 T172, CDKL3 prevents CDK4 from ubiquitin-
551 proteasomal degradation in cancer cells, thus preserving sufficient amount of CDK4
552 for G1 phase “highway” racing. Though phosphorylation of T172 was uncovered
553 previously as a demonstration of CDK4 activation (32, 33), the underlying
554 mechanism remained obscure. It was found in this work that phosphorylation of T172
555 can stabilize CDK4 by precluding the recognition of E3 ubiquitin ligase including
556 UBE3A, Stub1 and Trim28. Among them, Trim28 is identified as an E3 ligase of
557 CDK4 in this work, which causes the K48-linked poly-ubiquitination of CDK4 in the
558 absence of T172 phosphorylation.
559
560 As a member of CDKL kinase subfamily, the functional and molecular understandings
561 of CDKL3 are both under-explored. We have provided direct evidence that CDKL
562 kinase can enter the nucleus and function inside. Also, we discovered that the
563 conserved putative cyclin-binding α-helix on CDKL kinase in fact binds to cyclins and
564 is functionally required. After rational design and synthesis, we also presented the
565 potent CDKL3 inhibitor HZ1 for cancer treatment. This inhibitor is first-in-class, and
566 has very low dosage requirement in cancer growth repression both in vitro and in

vivo. After testing on patient-derived samples, we believe that HZ1 genuinely provides a promising perspective in cancer therapy. HZ1 can also be used together with other inhibitors as combinatory therapy and more importantly, may overcome the resistance of CDK4/6 inhibitors.

For future direction, the functional importance can be strengthened by transgenic animals. In a separate study, we have generated the *Cdkl3* flox mice and discovered the important role of *Cdkl3* in fatty liver diseases. We are generating the cancer model mice with the conditional-knockout of *Cdkl3* to validate the cell-cycle promoting effect of CDKL3. Also, how CDKL3 is regulated appears very intriguing to us, which is the next goal to pursue. And further design and tests of CDKL3 inhibitors based on HZ1 should be conducted for higher potency and specificity. Possible off-target effect of these molecules should be carefully examined in the preclinical models.

## Methods

### Sex as a biological variant

In this study, sex was not considered as a biological variable.

### Cell lines

This study used HEK293T (ATCC, Cat#CRL-11268), U2OS (ATCC, Cat#HTB-96), DLD-1 (NCACC, China, Cat#TCHu134), HeLa (ATCC, Cat#CCL-2), MDA-MB-231 (ATCC, Cat#HTB-26), MCF-7 (ATCC, Cat#HTB-22) and T47D (ATCC, Cat#HTB-133)

cells. All cell lines (parental and genetically modified) were cultured in DMEM (Gibco) medium supplemented with 10% FBS (fetal bovine serum) and 100 mg/mL of penicillin/streptomycin/glutamine (Gibco) in humidified incubators with 5% $CO_2$ at 37°C. All cell information is listed in Supplemental Table 2.

**Animal work and treatment**

BALB/cA-nude mice (Strain NO 13001A) were purchased from Beijing HFK Bioscience CO.,LTD. C57BL/6J WT (Strain NO.N000013) and C57BL/6J *Apc*$^{min/+}$ mice (Strain NO.T001457) were purchased from GemPharmatech (Nanjing, China). The nucleotides encoding the 850th amino acid of *Apc* gene was mutated to a stop codon, resulting in early termination of translation. After crossing with C57BL/6J WT mice, we generated mice with the genotype *Apc*$^{+/+}$ and *Apc*$^{min/+}$ . The example of mouse genotyping is showed in Supplemental Figure 7L, and the primers are listed in the Supplemental Table 2.

**Antibodies and immunoblotting**

Cells were prepared by PLB as described above and resuspended in SDS loading buffer, boiled at 95°C for 5 minutes to prepare protein samples. Protein samples were separated by using 6%-10% SDS-PAGE gels and PVDF membranes (Millipore) was used to transfer. Then, PVDF membranes were blocked in 3% BSA which was diluted with TBS-T buffer and incubated with indicated primary antibodies at 1:1,000 dilution overnight at 4°C. After 3 times washing by TBS-T for 10 minutes each time, the membranes were treated with corresponding secondary antibodies at 1:5,000 dilution at room temperature (RT) for 45 minutes. Before exposure, the membranes

were washed 3 times by TBS-T buffer for 10 minutes each time. The Tanon chemiluminescent substrate kit and Tanon 5200 Chemiluminescence Imaging System were used. Protein levels were quantified by ImageJ. All antibody information is listed in Supplemental Table 2. The polyclonal CDKL3 antibody was customized and produced by ABclonal. All other antibodies are commercial.

**Statistics**

Image J was used to quantify the results of immunoblotting, BrdU immunofluorescence and colony formation assay. GraphPad Prism 8.0 software was used for statistical analyses. BrdU immunofluorescence results analysis: 3 fields were randomly selected and about 100 cells were counted per field to calculate the proportion of BrdU-positive cells and mean BrdU intensity per cell. Experimental results were shown as the mean ± SD and n value of each set was indicated in the panel. One-way ANOVA was performed for statistical analysis. Flow cytometry results analysis: The analysis was performed using FlowJo version 10.0.7r2. Experimental results were shown as the mean ± SD, n=3 replicates, and two-tailed Student's t test (if 2 sets of data) or one-way ANOVA (if 3 or more sets) was performed for statistical analysis. Protein immunoblotting results quantification: The results of immunoblotting results were quantified with Image J. The protein expression values in CHX-blocking assay were normalized to those of GAPDH or tubulin. The protein expression values of pRb were normalized to those of Rb. Two-tailed Student's t test was performed for statistical analysis. MTT assay: The $OD_{490}$ values at each time point was plotted in Prism. Experimental results are shown as the mean ± SD, n=3 replicates, and two-

way ANOVA was performed for statistical analysis. Quantitative real-time PCR (RT-qPCR): The gene expression values were normalized to those of GAPDH. And data processing was performed using the $2^{-\Delta\Delta Ct}$ method. Experimental results are shown as the mean ± SD, n=3 replicates, and one-way ANOVA was performed for statistical analysis. Colony number: Used Image J to analyze the colony formation results. Experimental results are shown as the mean ± SD, n=3 replicates, and one-way ANOVA was performed for statistical analysis. Tumor volumes of athymic nude mouse : Tumor volume was calculated using the formula: ½ (Length × $Width^2$). Images were drawn after obtaining the tumor volumes in combination with the corresponding time points. Experimental results are shown as the mean ± SD, n=10, and two-way ANOVA was performed for statistical analysis. Tumor weight of athymic nude mouse: The tumor weight was measured after sacrificing the nude mice and dissecting the tumor. Images were drawn based on the weight results. Experimental results are shown as the mean ± SD, n=10, and two-tailed Student's t-test (if 2 sets of data) or one-way ANOVA (if 3 sets) was performed for statistical analysis. Tumor number and volume in the intestines of *Apc*$^{min/+}$ mice : After the end of experiment, the intestines of *Apc*$^{min/+}$ mice under different treatment were removed. The number and volume of different groups were recorded and measured. For tumor number, experimental results are shown as means ± SD , n=5 per group, by one-way ANOVA analysis. For tumor volume, experimental results are shown as means ± SD, by one-way ANOVA analysis. *Apc*$^{+/+}$+PBS group, n=3; *Apc*$^{min/+}$+PBS group, n=71; *Apc*$^{min/+}$+C3I-22 group, n=10. Superplot analysis was performed according to the

instruction (63). Semi-quantitative scoring of immunohistochemistry results: Experimental results are shown as the mean ± SD, n=5 replicates, and two-tailed Student's t test was performed for statistical analysis. The transcriptome database analysis: The expressions of CDKL3 mRNA level were acquired from TNMplot (60) and TCGA datasets. After normalized, P values were tested with Student's t-test or one-way ANOVA with post hoc Tukey's H SEM test between groups using GraphPad Prism 8. As shown in Figure 10A, Left: normal n=41, cancer n=282; Middle: normal n=41, cancer n=41; Right: normal n=377, cancer n=1450, metastatic n=99. Analysis of the expression correlation of CDKL3 with CDK4 and pRb: Immunohistochemistry scores were used for correlation analysis by two-tailed Spearman correlation, n=5. p values < 0.05 were considered to be statistically significant.

**Study Approval**

The procedures performed on patient tissue samples including organoid culturing and immunohistochemistry staining were in accordance with the ethical standards of EC-2023-KS-O43 (China Medical University). Written informed consent of the patient was received prior to participation. The general patient information is listed in Supplemental Table 1.

Production of mice and all research protocols in the study were approved by the Institutional Animal Care and Use Committee (IACUC) of Northeastern University under protocol number NEU-EC-2022A019S and NEU-EC-2022A048. In this study, all animals received humane care according to the criteria outlined in the "Guide for the Care and Use of Laboratory Animals".

## Data availability

All data is available in this manuscript. All materials are available upon reasonable request from the authors. All the data used to generate graphs are provided in the Supporting Data Values file.

## Author Contributions

R.S. and S.W. designed this study. H.Z., J.L., S.Z., L.M., Z.P., H.Y., C.M., Y.W., Q.H. and Z.L. performed the experiments and analyzed the data. X.Z., L.C., L.L., T.F., D.G., L.Y., X.P., C.D., S.W. and R.S. wrote and revised the manuscript. S.W. and R.S. oversaw this project. H.Z. focused on the mechanistic study and J.L. focused on the biology, who share equal contribution as co-first authors. H.Z. started and followed through the whole study and J.L. joined the study two years later than H.Z. Hence, H.Z. is placed in front of J.L.

**Acknowledgement**

The authors acknowledge Dr. Chao Zhao (Jilin University) for advice on the organic synthesis. R.S. acknowledges support by the Fundamental Research Fund for the Central Universities, China N182005006 (completed) and N2420001, the Starting Funds for 100-talent plan of Northeastern University, National Natural Science Foundation of China 31970721 and 81902830 (completed), and Liaoning Revitalization Talents Program XLYC1807239 (completed). S.W. acknowledges the support by National Natural Science Foundation of China 52073274. C.D. acknowledges the support by National Natural Science Foundation of China 32270205.

## References


1. Liu L, Michowski W, Kolodziejczyk A, and Sicinski P. The cell cycle in stem cell proliferation, pluripotency and differentiation. *Nature cell biology.* 2019;21(9):1060-7.
2. Malumbres M, and Barbacid M. Cell cycle, CDKs and cancer: a changing paradigm. *Nat Rev Cancer.* 2009;9(3):153-66.
3. Lim S, and Kaldis P. Cdks, cyclins and CKIs: roles beyond cell cycle regulation. *Development.* 2013;140(15):3079-93.
4. Satyanarayana A, and Kaldis P. Mammalian cell-cycle regulation: several Cdks, numerous cyclins and diverse compensatory mechanisms. *Oncogene.* 2009;28(33):2925-39.
5. Suski JM, Ratnayeke N, Braun M, Zhang T, Strmiska V, Michowski W, et al. CDC7-independent G1/S transition revealed by targeted protein degradation. *Nature.* 2022;605(7909):357-65.
6. Weintraub SJ, Chow KNB, Luo RX, Zhang SH, He S, and Dean DC. Mechanism of Active Transcriptional Repression by the Retinoblastoma Protein. *Nature.* 1995;375(6534):812-5.
7. Matthews HK, Bertoli C, and de Bruin RAM. Cell cycle control in cancer. *Nature reviews Molecular cell biology.* 2022;23(1):74-88.
8. Ren S, and Rollins BJ. Cyclin C/cdk3 promotes Rb-dependent G0 exit. *Cell.* 2004;117(2):239-51.
9. Tomas-Loba A, Manieri E, Gonzalez-Teran B, Mora A, Leiva-Vega L, Santamans AM, et al. p38 gamma is essential for cell cycle progression and liver tumorigenesis.

*Nature.* 2019;568(7753):557-+.

10. Kim MJ, Cervantes C, Jung YS, Zhang XS, Zhang J, Lee SH, et al. PAF remodels the DREAM complex to bypass cell quiescence and promote lung tumorigenesis. *Molecular cell.* 2021;81(8):1698-+.

11. Otto T, and Sicinski P. Cell cycle proteins as promising targets in cancer therapy. *Nat Rev Cancer.* 2017;17(2):93-115.

12. Zhang M, Zhang L, Hei R, Li X, Cai H, Wu X, et al. CDK inhibitors in cancer therapy, an overview of recent development. *Am J Cancer Res.* 2021;11(5):1913-35.

13. Goel S, Bergholz JS, and Zhao JJ. Targeting CDK4 and CDK6 in cancer. *Nat Rev Cancer.* 2022;22(6):356-72.

14. Haq R, Randall S, Midmer M, Yee K, and Zanke B. NKIATRE is a novel conserved cdc2-related kinase. *Genomics.* 2001;71(2):131-41.

15. Yee KWL, Moore SJ, Midmer M, Zanke BW, Tong F, Hedley D, et al. NKIAMRE, a novel conserved CDC2-related kinase with features of both mitogen-activated protein kinases and cyclin-dependent kinases. *Biochem Bioph Res Co.* 2003;308(4):784-92.

16. Midmer M, Haq R, Squire JA, and Zanke BW. Identification of NKIAMRE, the human homologue to the mitogen-activated protein kinase-/cyclin-dependent kinase-related protein kinase NKIATRE, and its loss in leukemic blasts with chromosome arm 5q deletion. *Cancer research.* 1999;59(16):4069-74.

17. Zhu YC, and Xiong ZQ. Molecular and Synaptic Bases of CDKL5 Disorder. *Dev Neurobiol.* 2019;79(1):8-19.

18. Park K, Li C, Tsiropoulou S, Goncalves J, Kondratev C, Pelletier L, et al. CDKL kinase

regulates the length of the ciliary proximal segment. *Curr Biol.* 2021;31(11):2359-73 e7.

19. Canning P, Park K, Goncalves J, Li C, Howard CJ, Sharpe TD, et al. CDKL Family Kinases Have Evolved Distinct Structural Features and Ciliary Function. *Cell reports.* 2018;22(4):885-94.

20. Cui Y, Yang Z, Wang H, Yan Y, Huang Q, Gong Z, et al. Identification of CDKL3 as a critical regulator in development of glioma through regulating RRM2 and the JNK signaling pathway. *Cancer Sci.* 2021;112(8):3150-62.

21. He A, Ma L, Huang Y, Zhang H, Duan W, Li Z, et al. CDKL3 promotes osteosarcoma progression by activating Akt/PKB. *Life Sci Alliance.* 2020;3(5).

22. Ye W, Zhu J, He D, Yu D, Yang H, Wang W, et al. Increased CDKL3 expression predicts poor prognosis and enhances malignant phenotypes in esophageal squamous cell carcinoma. *J Cell Biochem.* 2019;120(5):7174-84.

23. Leif RC, Stein JH, and Zucker RM. A short history of the initial application of anti-5-BrdU to the detection and measurement of S phase. *Cytom Part A.* 2004;58a(1):45-52.

24. Pardee AB. A restriction point for control of normal animal cell proliferation. *Proceedings of the National Academy of Sciences of the United States of America.* 1974;71(4):1286-90.

25. Lee S, Micalizzi D, Truesdell SS, Bukhari SIA, Boukhali M, Lombardi-Story J, et al. A post-transcriptional program of chemoresistance by AU-rich elements and TTP in quiescent leukemic cells. *Genome Biol.* 2020;21(1):33.

768 26. Sosa MS, Parikh F, Maia AG, Estrada Y, Bosch A, Bragado P, et al. NR2F1 controls
769 tumour cell dormancy via SOX9- and RARbeta-driven quiescence programmes.
770 *Nature communications.* 2015;6:6170.
771 27. Liu PD, Begley M, Michowski W, Inuzuka H, Ginzberg M, Gao DM, et al. Cell-cycle-
772 regulated activation of Akt kinase by phosphorylation at its carboxyl terminus. *Nature.*
773 2014;508(7497):541-+.
774 28. Adams PD, Sellers WR, Sharma SK, Wu AD, Nalin CM, and Kaelin WG. Identification
775 of a cyclin-cdk2 recognition motif present in substrates and p21-like cyclin-dependent
776 kinase inhibitors. *Molecular and cellular biology.* 1996;16(12):6623-33.
777 29. Sellers WR, Rodgers JW, and Kaelin WG. A Potent Transrepression Domain in the
778 Retinoblastoma Protein Induces a Cell-Cycle Arrest When Bound to E2f Sites.
779 *Proceedings of the National Academy of Sciences of the United States of America.*
780 1995;92(25):11544-8.
781 30. Harbour JW, Luo RX, Santi AD, Postigo AA, and Dean DC. Cdk phosphorylation
782 triggers sequential intramolecular interactions that progressively block Rb functions
783 as cells move through G1. *Cell.* 1999;98(6):859-69.
784 31. Swatek KN, and Komander D. Ubiquitin modifications. *Cell research.* 2016;26(4):399-
785 422.
786 32. Schachter MM, Merrick KA, Larochelle S, Hirschi A, Zhang C, Shokat KM, et al. A
787 Cdk7-Cdk4 T-loop phosphorylation cascade promotes G1 progression. *Molecular cell.*
788 2013;50(2):250-60.
789 33. Bockstaele L, Bisteau X, Paternot S, and Roger PP. Differential regulation of cyclin-

dependent kinase 4 (CDK4) and CDK6, evidence that CDK4 might not be activated by CDK7, and design of a CDK6 activating mutation. *Molecular and cellular biology.* 2009;29(15):4188-200.

34. Yu Q, Sicinska E, Geng Y, Ahnstrom M, Zagozdzon A, Kong Y, et al. Requirement for CDK4 kinase function in breast cancer. *Cancer Cell.* 2006;9(1):23-32.

35. Klier M, Anastasov N, Hermann A, Meindl T, Angermeier D, Raffeld M, et al. Specific lentiviral shRNA-mediated knockdown of cyclin D1 in mantle cell lymphoma has minimal effects on cell survival and reveals a regulatory circuit with cyclin D2. *Leukemia.* 2008;22(11):2097-105.

36. Chen B, and Pollard JW. Cyclin D2 compensates for the loss of cyclin D1 in estrogen-induced mouse uterine epithelial cell proliferation. *Mol Endocrinol.* 2003;17(7):1368-81.

37. Zhang Q, Sakamoto K, Liu CB, Triplett AA, Lin WC, Rui H, et al. Cyclin D3 Compensates for the Loss of Cyclin D1 during ErbB2-Induced Mammary Tumor Initiation and Progression. *Cancer research.* 2011;71(24):7513-24.

38. Bhuripanyo K, Wang Y, Liu X, Zhou L, Liu R, Duong D, et al. Identifying the substrate proteins of U-box E3s E4B and CHIP by orthogonal ubiquitin transfer. *Science advances.* 2018;4(1):e1701393.

39. Wang Y, Liu X, Zhou L, Duong D, Bhuripanyo K, Zhao B, et al. Identifying the ubiquitination targets of E6AP by orthogonal ubiquitin transfer. *Nature communications.* 2017;8(1):2232.

40. Jang SM, Kauzlaric A, Quivy JP, Pontis J, Rauwel B, Coluccio A, et al. KAP1

facilitates reinstatement of heterochromatin after DNA replication. *Nucleic Acids Res.* 2018;46(17):8788-802.

41. Huang ZL, Li X, Tang B, Li H, Zhang JN, Sun R, et al. SETDB1 Modulates Degradation of Phosphorylated RB and Anticancer Efficacy of CDK4/6 Inhibitors. *Cancer research.* 2023;83(6).

42. Rousseaux MWC, de Haro M, Lasagna-Reeves CA, De Maio A, Park J, Jafar-Nejad P, et al. TRIM28 regulates the nuclear accumulation and toxicity of both alpha-synuclein and tau. *eLife.* 2016;5.

43. Zhang RY, Liu ZK, Wei D, Yong YL, Lin P, Li H, et al. UBE2S interacting with TRIM28 in the nucleus accelerates cell cycle by ubiquitination of p27 to promote hepatocellular carcinoma development. *Signal Transduct Target Ther.* 2021;6(1):64.

44. Watanabe M, Saeki Y, Takahashi H, Ohtake F, Yoshida Y, Kasuga Y, et al. A substrate-trapping strategy to find E3 ubiquitin ligase substrates identifies Parkin and TRIM28 targets. *Commun Biol.* 2020;3(1):592.

45. Lin RH, Connolly PJ, Huang SL, Wetter SK, Lu YH, Murray WV, et al. 1-acyl-1H-[1,2,4]triazole-3,5-diamine analogues as novel and potent anticancer cyclin-dependent kinase inhibitors: Synthesis and evaluation of biological activities. *J Med Chem.* 2005;48(13):4208-11.

46. Chen G, and Deng X. Cell Synchronization by Double Thymidine Block. *Bio Protoc.* 2018;8(17).

47. Toogood PL, Harvey PJ, Repine JT, Sheehan DJ, VanderWel SN, Zhou HR, et al. Discovery of a potent and selective inhibitor of cyclin-dependent kinase 4/6. *J Med*

*Chem.* 2005;48(7):2388-406.

48. Bollard J, Miguela V, de Galarreta MR, Venkatesh A, Bian CB, Roberto MP, et al. Palbociclib (PD-0332991), a selective CDK4/6 inhibitor, restricts tumour growth in preclinical models of hepatocellular carcinoma. *Gut.* 2017;66(7):1286-96.

49. Comstock CES, Augello MA, Goodwin JF, de Leeuw R, Schiewer MJ, Ostrander WF, et al. Targeting cell cycle and hormone receptor pathways in cancer. *Oncogene.* 2013;32(48):5481-91.

50. Statsuk AV, Maly DJ, Seeliger MA, Fabian MA, Biggs WH, 3rd, Lockhart DJ, et al. Tuning a three-component reaction for trapping kinase substrate complexes. *J Am Chem Soc.* 2008;130(51):17568-74.

51. Beaver JA, Amiri-Kordestani L, Charlab R, Chen W, Palmby T, Tilley A, et al. FDA Approval: Palbociclib for the Treatment of Postmenopausal Patients with Estrogen Receptor-Positive, HER2-Negative Metastatic Breast Cancer. *Clin Cancer Res.* 2015;21(21):4760-6.

52. Sumi NJ, Kuenzi BM, Knezevic CE, Rix LLR, and Rix U. Chemoproteomics Reveals Novel Protein and Lipid Kinase Targets of Clinical CDK4/6 Inhibitors in Lung Cancer. *Acs Chem Biol.* 2015;10(12):2680-6.

53. Rihani A, Vandesompele J, Speleman F, and Van Maerken T. Inhibition of CDK4/6 as a novel therapeutic option for neuroblastoma. *Cancer Cell Int.* 2015;15.

54. Wardell SE, Ellis MJ, Alley HM, Eisele K, VanArsdale T, Dann SG, et al. Efficacy of SERD/SERM Hybrid-CDK4/6 Inhibitor Combinations in Models of Endocrine Therapy-Resistant Breast Cancer. *Clinical Cancer Research.* 2015;21(22):5121-30.

55. Li ZH, Wang XH, Eksterowicz J, Gribble MW, Alba GQ, Ayres M, et al. Discovery of AMG 925, a FLT3 and CDK4 Dual Kinase Inhibitor with Preferential Affinity for the Activated State of FLT3. *J Med Chem.* 2014;57(8):3430-49.

56. AbuHammad S, Cullinane C, Martin C, Bacolas Z, Ward T, Chen HQ, et al. Regulation of PRMT5-MDM4 axis is critical in the response to CDK4/6 inhibitors in melanoma. *Proceedings of the National Academy of Sciences of the United States of America.* 2019;116(36):17990-8000.

57. Dang F, Nie L, Zhou J, Shimizu K, Chu C, Wu Z, et al. Inhibition of CK1epsilon potentiates the therapeutic efficacy of CDK4/6 inhibitor in breast cancer. *Nature communications.* 2021;12(1):5386.

58. Burtin F, Mullins CS, and Linnebacher M. Mouse models of colorectal cancer: Past, present and future perspectives. *World J Gastroentero.* 2020;26(13):1394-426.

59. Wang XM, Yang C, Zhao Y, Xu ZG, Yang W, Wang P, et al. The deubiquitinase USP25 supports colonic inflammation and bacterial infection and promotes colorectal cancer. *Nat Cancer.* 2020;1(8):811-+.

60. Bartha A, and Gyorffy B. TNMplot.com: A Web Tool for the Comparison of Gene Expression in Normal, Tumor and Metastatic Tissues. *International Journal of Molecular Sciences.* 2021;22(5).

61. Lanczky A, and Gyorffy B. Web-Based Survival Analysis Tool Tailored for Medical Research (KMplot): Development and Implementation. *J Med Internet Res.* 2021;23(7).

62. van de Wetering M, Francies HE, Francis JM, Bounova G, Iorio F, Pronk A, et al.

Prospective derivation of a living organoid biobank of colorectal cancer patients. *Cell.* 2015;161(4):933-45.

63. Lord SJ, Velle KB, Mullins RD, and Fritz-Laylin LK. SuperPlots: Communicating reproducibility and variability in cell biology. *Journal of Cell Biology.* 2020;219(6).

# Figure 1

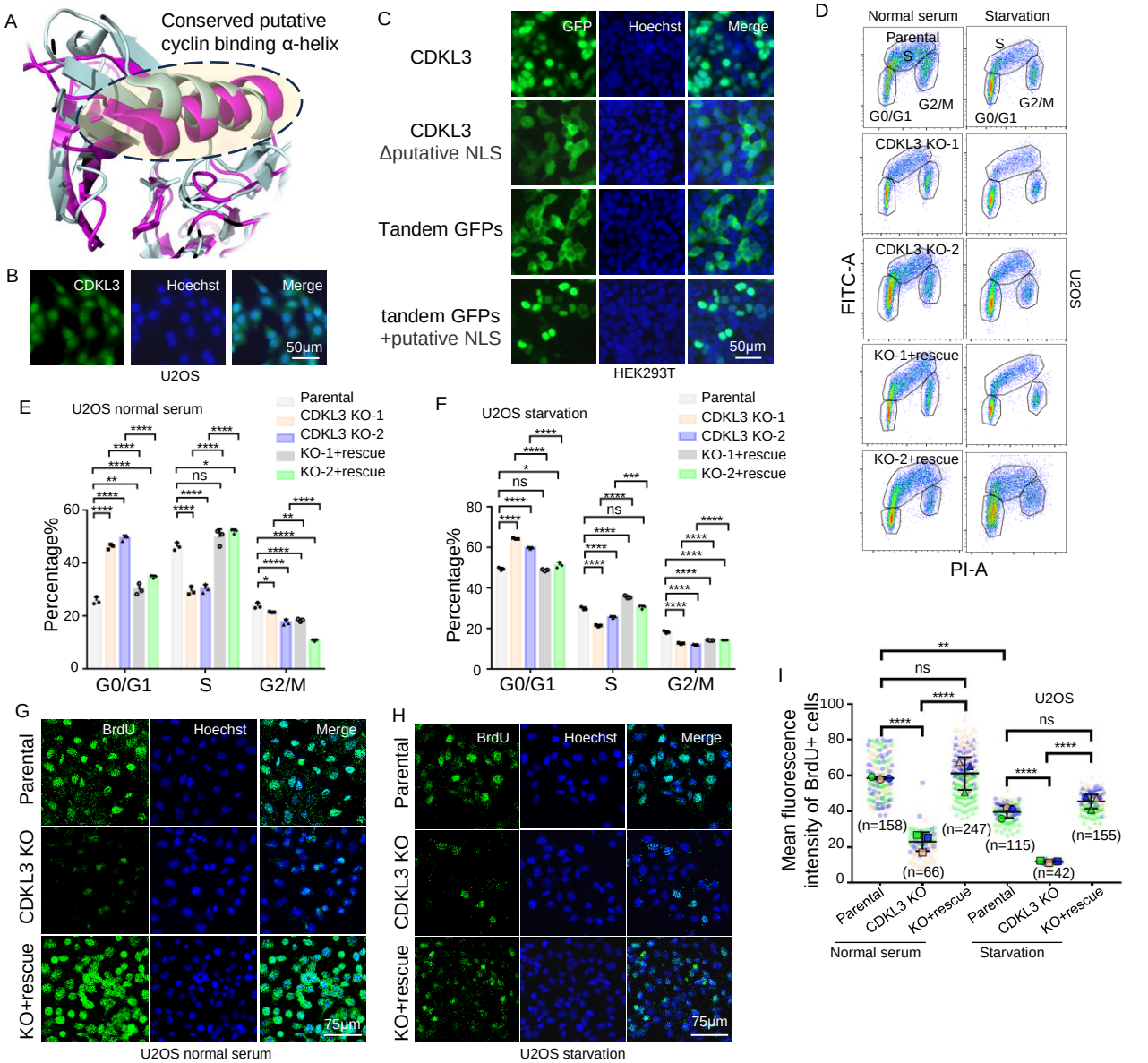
A
Conserved putative
cyclin binding α-helix
B
CDKL3
Hoechst
Merge
50μm
U2OS
C
GFP
Hoechst
Merge
CDKL3
CDKL3
Δputative NLS
Tandem GFPs
tandem GFPs
+putative NLS
50μm
HEK293T
D
Normal serum
Starvation
Parental
CDKL3 KO-1
CDKL3 KO-2
KO-1+rescue
KO-2+rescue
G0/G1
S
G2/M
FITC-A
PI-A
U2OS
E
U2OS normal serum
Parental
CDKL3 KO-1
CDKL3 KO-2
KO-1+rescue
KO-2+rescue
Percentage%
G0/G1
S
G2/M
F
U2OS starvation
G
BrdU
Hoechst
Merge
Parental
CDKL3 KO
KO+rescue
75μm
U2OS normal serum
H
U2OS starvation
I
Mean fluorescence
intensity of BrdU+ cells
U2OS
(n=158)
(n=66)
(n=247)
(n=115)
(n=42)
(n=155)
Normal serum
Starvation

**Figure 1. CDKL3-loss causes cell cycle arrest in cancers.** (**A**) Overlay of the kinase domains of CDK1 (pale grey, PDBID: 4YC3) and CDKL3 (purple, PDBID: 3ZDU). (**B**) Immunostaining showing the nuclear-localization of endogenous CDKL3. (**C**) Fluorescent images of GFP-labeled proteins confirming the NLS function of CDKL3. (**D**) Representative flow cytometry results of U2OS cells with BrdU-FITC/Propidium Iodide (PI) dual staining. (**E, F**) Statistical analysis of the flow cytometry results in **D** showing CDKL3 ablation significantly increased G0/G1 percentage. Error bar means ± SD, n=3, by one-way ANOVA. CDKL3 KO-1 were abbreviated as CDKL3 KO in sequel experiments. (**G, H**) Representative immunofluorescent images of BrdU in U2OS cells under normal (**G**) or starvation (**H**) conditions. (**I**) Superplot analysis of the number of BrdU-positive cells and mean BrdU intensity per cell in **G** and **H**. Error bar means ± SD, triplicated, by one-way ANOVA. n value in the panel represents the total number of cells. All images in the same panel are under the same amplification scales. ns, not significant; *, $p<0.05$; **, $p<0.01$; ***, $p<0.001$; ****, $p<0.0001$.

# Figure 2

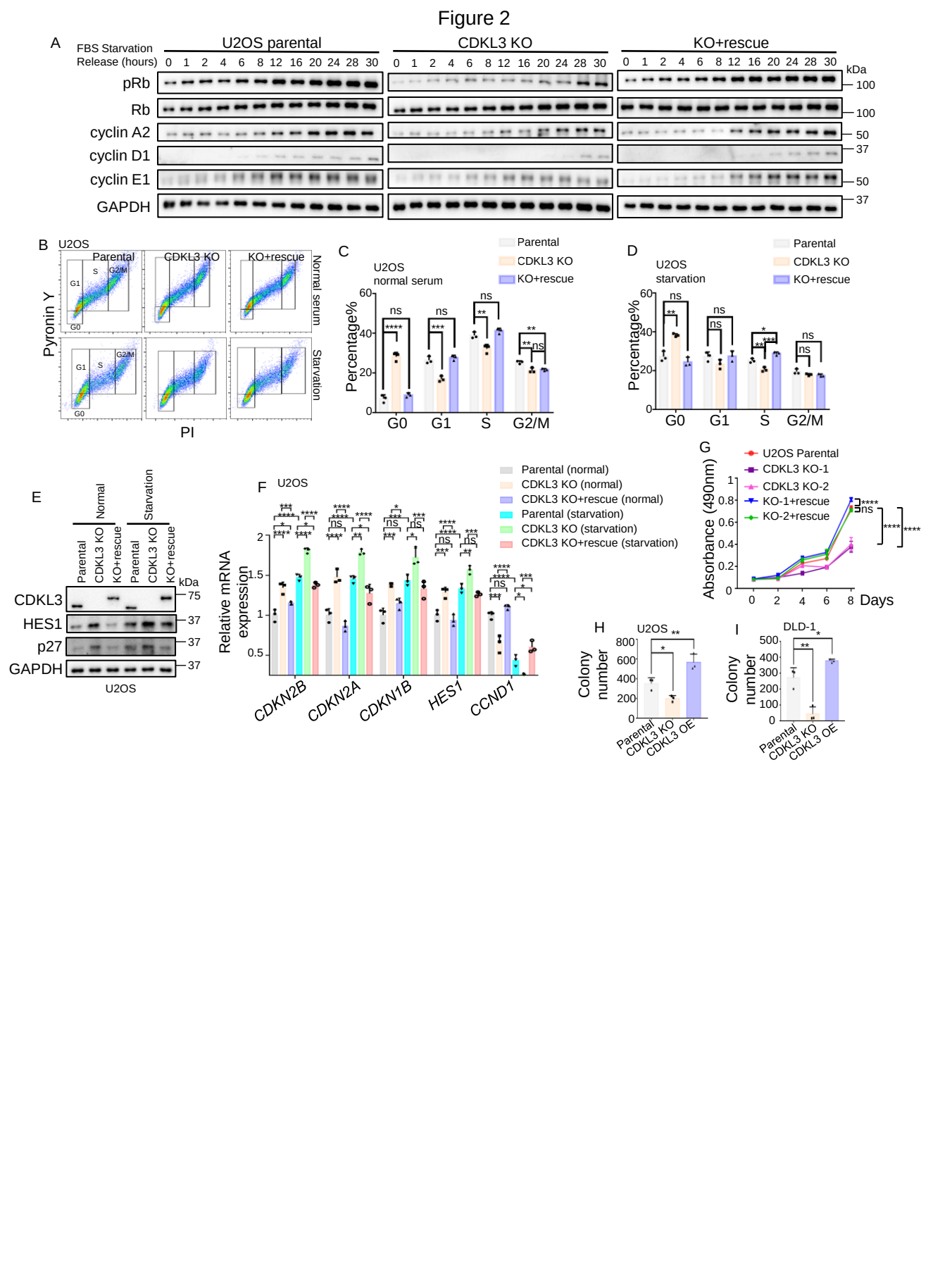
A
FBS Starvation
Release (hours)
U2OS parental
CDKL3 KO
KO+rescue
0 1 2 4 6 8 12 16 20 24 28 30
kDa
pRb
Rb
cyclin A2
cyclin D1
cyclin E1
GAPDH
100
100
50
37
50
37
B
U2OS
Parental
CDKL3 KO
KO+rescue
Normal serum
Starvation
Pyronin Y
PI
G1
S
G2/M
G0
C
U2OS
normal serum
Parental
CDKL3 KO
KO+rescue
Percentage%
G0
G1
S
G2/M
ns
D
U2OS
starvation
E
Normal
Starvation
Parental
CDKL3 KO
KO+rescue
CDKL3
HES1
p27
GAPDH
kDa
75
37
37
37
U2OS
F
U2OS
Parental (normal)
CDKL3 KO (normal)
CDKL3 KO+rescue (normal)
Parental (starvation)
CDKL3 KO (starvation)
CDKL3 KO+rescue (starvation)
Relative mRNA expression
CDKN2B
CDKN2A
CDKN1B
HES1
CCND1
G
U2OS Parental
CDKL3 KO-1
CDKL3 KO-2
KO-1+rescue
KO-2+rescue
Absorbance (490nm)
Days
H
U2OS
Colony number
Parental
CDKL3 KO
CDKL3 OE
I
DLD-1
Colony number
Parental
CDKL3 KO
CDKL3 OE

**Figure 2. CDKL3-loss retards cancer cell growth by impeding G0-to-G1 transition.** (**A**) Immunoblotting of multiple cell cycle related proteins after serum starvation and release. pRb: pS807/pS811 Rb. (**B**) Representative flow cytometry results of U2OS cells with Pyronin Y/PI dual staining. (**C, D**) Statistical analysis of **B** showing CDKL3 ablation significantly increased G0 proportion. Error bar means ± SD, n=3, by one-way ANOVA. (**E**) Immunoblotting showing CDKL3 ablation or starvation increased the protein levels of G0 markers, HES1 and p27, in U2OS cells. (**F**) RT-pPCR assay showing the transcription of G0 markers genes (*CDKN2B*, *CDKN2A*, *CDKN1B* and *HES1*) increased in the absence of CDKL3 in U2OS cells. *CCND1* was used as the marker of G1 phase. Error bar means ± SD, n=3, by one-way ANOVA. (**G**) MTT assay showing the growth of U2OS cells. Error bars mean ± SD, n=3, two-way ANOVA. (**H, I**) Statistical analyses of the colony numbers under three-dimensional culturing of U2OS (**H**) and DLD-1 (**I**) cells. Error bar means ± SD, n=3, by one-way ANOVA. ns, not significant; *, $p<0.05$; **, $p<0.01$; ***, $p<0.001$; ****, $p<0.0001$.

# Figure 3

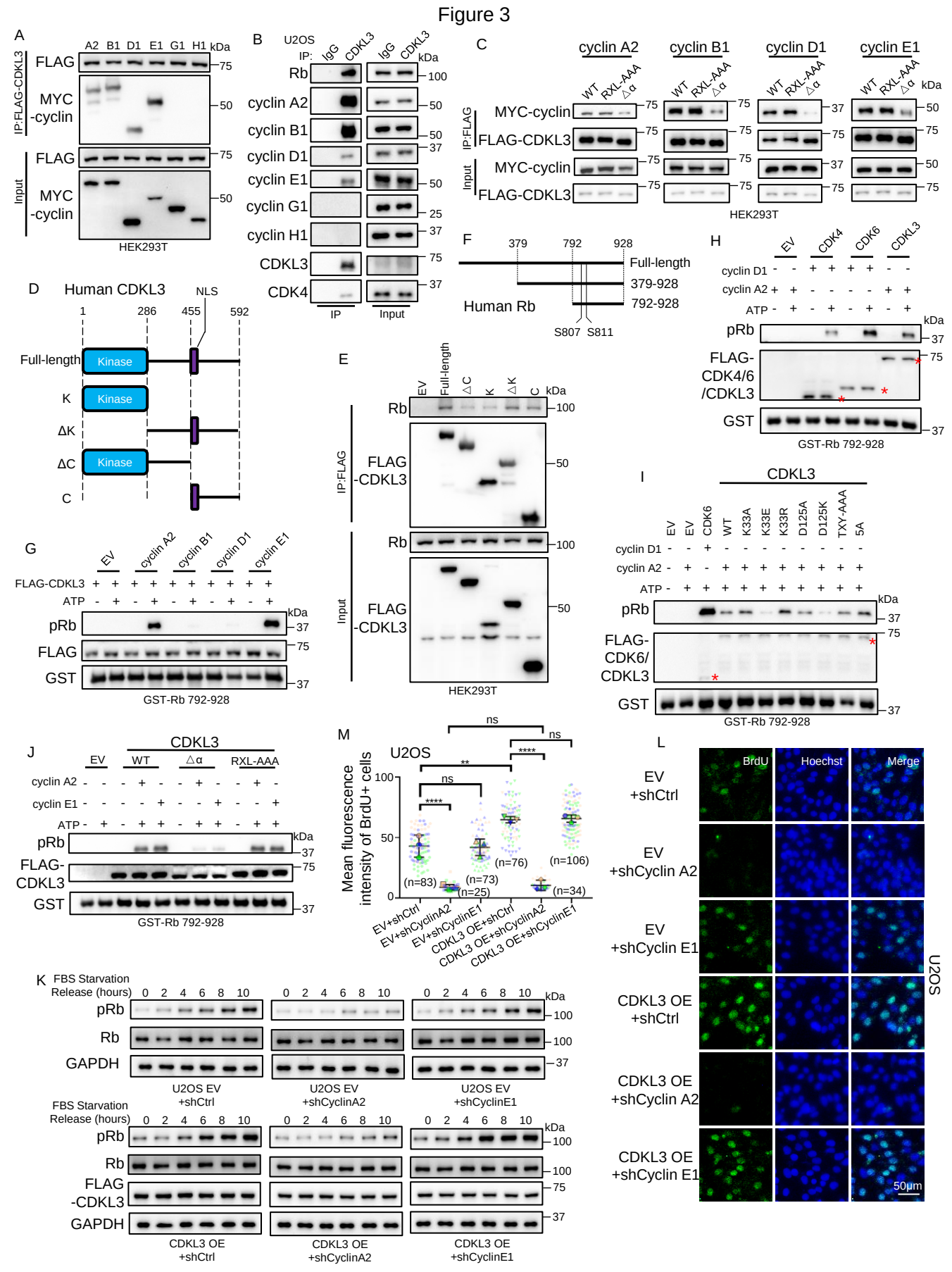
A
A2 B1 D1 E1 G1 H1 kDa
IP:FLAG-CDKL3
FLAG
MYC -cyclin
Input
HEK293T
B
U2OS
IP: IgG CDKL3 IgG CDKL3
Rb
cyclin A2
cyclin B1
cyclin D1
cyclin E1
cyclin G1
cyclin H1
CDKL3
CDK4
IP
Input
C
cyclin A2
cyclin B1
cyclin D1
cyclin E1
WT RXL-AAA △α
IP:FLAG
MYC-cyclin
FLAG-CDKL3
Input
HEK293T
D
Human CDKL3
NLS
Full-length
K
ΔK
ΔC
C
Kinase
E
EV Full-length △C K △K C
IP:FLAG
Input
HEK293T
F
Human Rb
Full-length
379-928
792-928
S807 S811
G
EV cyclin A2 cyclin B1 cyclin D1 cyclin E1
FLAG-CDKL3
ATP
pRb
FLAG
GST
GST-Rb 792-928
H
EV CDK4 CDK6 CDKL3
cyclin D1
cyclin A2
ATP
pRb
FLAG-CDK4/6 /CDKL3
GST
GST-Rb 792-928
I
CDKL3
EV EV CDK6 WT K33A K33E K33R D125A D125K TXY-AAA 5A
cyclin D1
cyclin A2
ATP
pRb
FLAG-CDK6/ CDKL3
GST
GST-Rb 792-928
J
CDKL3
EV WT △α RXL-AAA
cyclin A2
cyclin E1
ATP
pRb
FLAG-CDKL3
GST
GST-Rb 792-928
M
U2OS
Mean fluorescence intensity of BrdU+ cells
ns
**
****
(n=83)
(n=73)
(n=25)
(n=76)
(n=106)
(n=34)
EV+shCtrl
EV+shCyclinA2
EV+shCyclinE1
CDKL3 OE+shCtrl
CDKL3 OE+shCyclinA2
CDKL3 OE+shCyclinE1
L
BrdU Hoechst Merge
EV +shCtrl
EV +shCyclin A2
EV +shCyclin E1
CDKL3 OE +shCtrl
CDKL3 OE +shCyclin A2
CDKL3 OE +shCyclin E1
U2OS
50μm
K
FBS Starvation Release (hours) 0 2 4 6 8 10
pRb
Rb
GAPDH
U2OS EV +shCtrl
U2OS EV +shCyclinA2
U2OS EV +shCyclinE1
FLAG -CDKL3
CDKL3 OE +shCtrl
CDKL3 OE +shCyclinA2
CDKL3 OE +shCyclinE1

**Figure 3. CDKL3 phosphorylates Rb for cell cycle entry when coupling with cyclin A2.** (**A**) Co-IP assay showing exogenous CDKL3 binds to cyclin A2, B1, D1 and E1. (**B**) Co-IP assay showing endogenous CDKL3 binds to endogenous cyclin A2, B1, D1 and E1, as well as Rb and CDK4. (**C**) Co-IP assay showing the truncation of the putative cyclin binding α-helix on the kinase domain of CDKL3 (Δα) abrogated CDKL3 binding to cyclins. RXL-AAA: R148A/T149A/L150A/R510A/K511A/L512A. (**D**) Schematic drawing of the segments of CDKL3. (**E**) Co-IP assay showing the carboxyl region of CDKL3 binds to Rb. (**F**) Schematic drawing of the commonly-used segments of Rb in vitro. S807 and S811 are the major phosphorylation sites. (**G**) In vitro kinase assay showing CDKL3 phosphorylates Rb in the presence of cyclin A2 and E1. (**H**) In vitro kinase assay showing CDKL3 phosphorylates Rb to the similar extent of CDK4/6. (**I**) In vitro kinase assay showing CDKL3 K33E and D125K mutants lost the capacity to phosphorylate Rb. TXY-AAA: T158A/D159A/Y160A, 5A: K33A/D125A/T158A/D159A/Y160A. (**J**) In vitro kinase assay showing CDKL3 Δα mutant lost the capacity of Rb phosphorylation. (**K**) Immunoblotting assay showing CDKL3 promoted the initial Rb phosphorylation depending on cyclin A2 after serum starvation and release in U2OS cells. (**L**) Representative images of immunofluorescence of BrdU in U2OS cells. (**M**) Superplot analysis of the number of BrdU-positive cells and mean BrdU intensity per cell in **L**. Error bar means ± SD, triplicated, by one-way ANOVA. n value in the panel represents the total number of cells. ns, not significant; **, $p<0.01$; ****, $p<0.0001$. Red asterisks represent the target protein bands.

# Figure 4

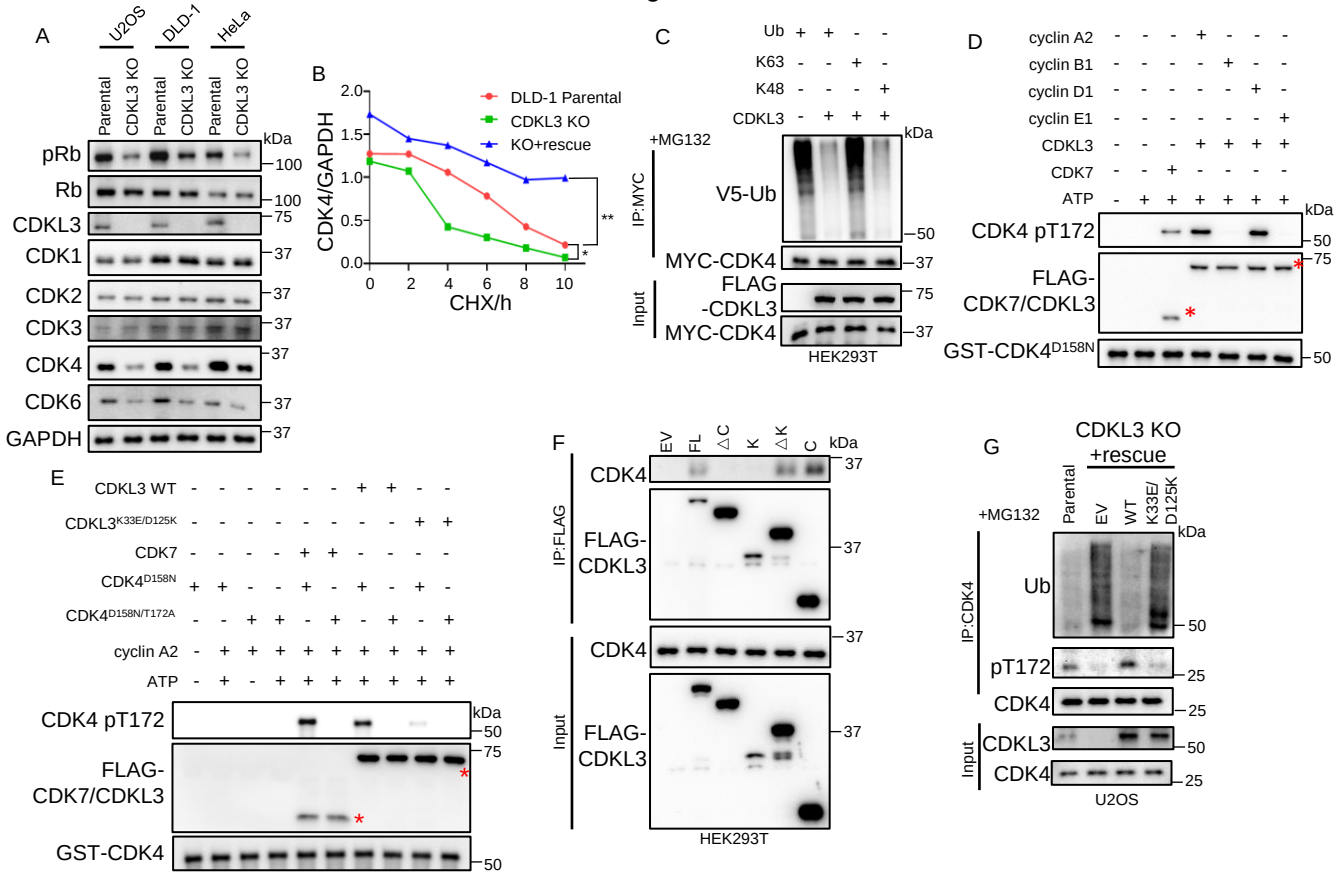
A
U2OS
DLD-1
HeLa
Parental
CDKL3 KO
kDa
pRb
Rb
CDKL3
CDK1
CDK2
CDK3
CDK4
CDK6
GAPDH
B
DLD-1 Parental
CDKL3 KO
KO+rescue
CDK4/GAPDH
CHX/h
C
Ub
K63
K48
CDKL3
+MG132
IP:MYC
V5-Ub
MYC-CDK4
Input
FLAG
-CDKL3
HEK293T
D
cyclin A2
cyclin B1
cyclin D1
cyclin E1
CDK7
ATP
CDK4 pT172
FLAG-
CDK7/CDKL3
GST-CDK4D158N
E
CDKL3 WT
CDKL3K33E/D125K
CDK7
CDK4D158N
CDK4D158N/T172A
cyclin A2
ATP
CDK4 pT172
FLAG-
CDK7/CDKL3
GST-CDK4
F
EV
FL
△C
K
△K
C
IP:FLAG
CDK4
FLAG-
CDKL3
Input
HEK293T
G
CDKL3 KO
+rescue
Parental
EV
WT
K33E/
D125K
+MG132
IP:CDK4
Ub
pT172
CDK4
Input
CDKL3
U2OS

**Figure 4. CDKL3 phosphorylates CDK4 on T172 to stabilize CDK4.** (**A**) CDKL3 knockout reduced the protein levels of endogenous CDK4 and CDK6 in multiple cell lines. The levels of CDK1/2/3 remained unaffected. (**B**) The CHX-blocking assay of endogenous CDK4 protein showing CDK4 protein stability was positively correlated with CDKL3 level. Error bar means ± SD, by one-way ANOVA (**C**) Ubiquitination assay of CDK4 showing the presence of CDKL3 specifically reduced K48-linked poly-ubiquitination of CDK4. K63: a Ub mutant with all Lys mutated to Arg except Lys63. K48: a Ub mutant with all Lys mutated to Arg except Lys48 (**D, E**) In vitro kinase assay showing CDKL3 phosphorylates CDK4 on T172 in the presence of cyclin A2 and D1 (**D**). And K33E/D125K mutant lost the capacity (**E**). The kinase-dead mutant of CDK4 (D158N) was used as substrate to avoid self-phosphorylation. (**F**) Co-IP assay revealing the carboxyl region of CDKL3 is primarily involved in CDK4 binding. (**G**) Ubiquitination assay of endogenous CDK4 in the presence of WT CDKL3 and K33E/D125K. K33E/D125K lost the capacity to reduce CDK4 ubiquitination. MG132 was pretreated to maintain the same protein level. Red asterisks represent the target protein bands. *, $p<0.05$; **, $p<0.01$.

# Figure 5

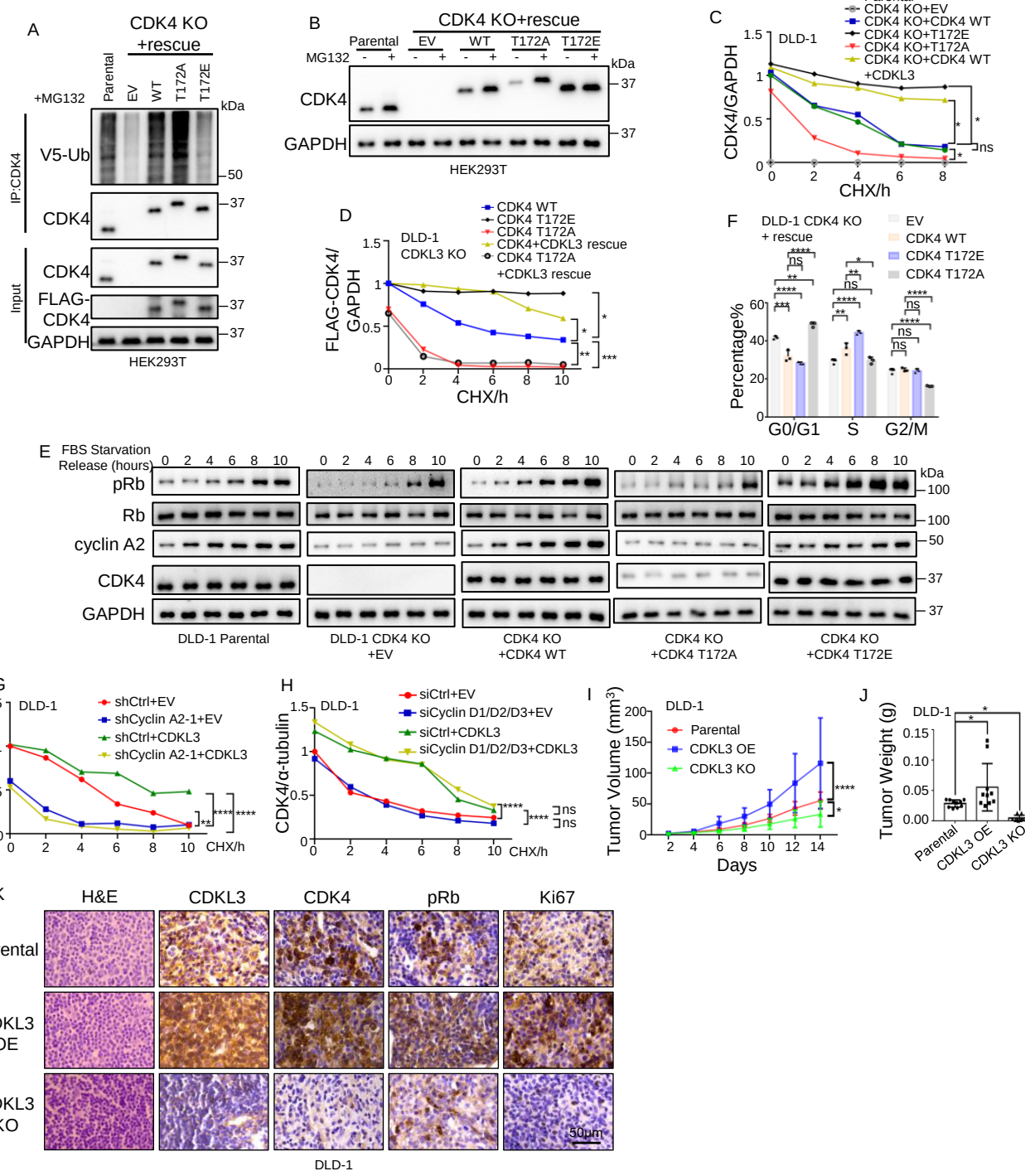
A
CDK4 KO +rescue
Parental
EV
WT
T172A
T172E
+MG132
kDa
IP:CDK4
V5-Ub
CDK4
Input
CDK4
FLAG-CDK4
GAPDH
HEK293T
B
CDK4 KO+rescue
Parental
EV
WT
T172A
T172E
MG132
CDK4
GAPDH
HEK293T
C
DLD-1
CDK4/GAPDH
CHX/h
Parental
CDK4 KO+EV
CDK4 KO+CDK4 WT
CDK4 KO+T172E
CDK4 KO+T172A
CDK4 KO+CDK4 WT +CDKL3
D
DLD-1 CDKL3 KO
FLAG-CDK4/GAPDH
CHX/h
CDK4 WT
CDK4 T172E
CDK4 T172A
CDK4+CDKL3 rescue
CDK4 T172A +CDKL3 rescue
F
DLD-1 CDK4 KO + rescue
Percentage%
G0/G1
S
G2/M
EV
CDK4 WT
CDK4 T172E
CDK4 T172A
E
FBS Starvation
Release (hours)
pRb
Rb
cyclin A2
CDK4
GAPDH
DLD-1 Parental
DLD-1 CDK4 KO +EV
CDK4 KO +CDK4 WT
CDK4 KO +CDK4 T172A
CDK4 KO +CDK4 T172E
G
DLD-1
CDK4/GAPDH
CHX/h
shCtrl+EV
shCyclin A2-1+EV
shCtrl+CDKL3
shCyclin A2-1+CDKL3
H
DLD-1
CDK4/α-tubulin
CHX/h
siCtrl+EV
siCyclin D1/D2/D3+EV
siCtrl+CDKL3
siCyclin D1/D2/D3+CDKL3
I
DLD-1
Tumor Volume (mm³)
Days
Parental
CDKL3 OE
CDKL3 KO
J
DLD-1
Tumor Weight (g)
Parental
CDKL3 OE
CDKL3 KO
K
H&E
CDKL3
CDK4
pRb
Ki67
Parental
CDKL3 OE
CDKL3 KO
50μm
DLD-1

**Figure 5. Phosphorylation on T172 prevents the ubiquitin-proteasomal degradation of CDK4 and secures the function of CDK4.** (**A**) Ubiquitination assay of CDK4 WT, T172A and T172E in CDK4 KO-and-rescued HEK293T cells. Ubiquitination was enhanced for T172A and reduced for T172E. MG132 was pretreated to maintain the same protein level. The rescue of CDK4 WT, T172A and T172E was approximately at the same level with the endogenous CDK4. (**B**) Immunoblotting assay showing MG132 treatment stabilizes CDK4 T172A in CDK4 KO-and-rescued HEK293T cells. CDK4 T172E was insensitive to MG132 treatment. (**C**) The CHX-blocking assay showing CDK4 T172E had high protein stability whereas T172A had low protein stability in CDK4 KO-and-rescued DLD-1 cells. (**D**) The CHX-blocking assay showing CDK4 T172E remained stable when CDKL3 was ablated. And the stability T172A was unaffected by CDKL3 presence. (**E**) Immunoblotting assay showing CDK4 T172A failed to promote high level of Rb phosphorylation after serum starvation and release in CDK4 KO-and-rescued DLD-1 cells. (**F**) Statistical analysis of the flow cytometry results showing CDK4 T172A failed to promote G1 phase progression. Error bar means ± SD, n=3, by one-way ANOVA. (**G, H**) The CHX-blocking assay showing the stabilization of CDK4 by CDKL3 was dependent on cyclin A2 (**G**) instead of cyclin D (**H**). (**I, J**) Quantitative analyses of the tumor volume (**I**) and weight (**J**) of tumors formed by the subcutaneously transplanted DLD-1 cells. (**I**): Error bars mean ± SD, n=10, two-way ANOVA. (**J**): Error bar means ± SD, n=10, by one-way ANOVA. (**K**) Representative IHC staining and hematoxylin-eosin staining images of subcutaneously transplanted DLD-1 cells. ns, not significant; *, $p<0.05$; **, $p<0.01$; ***, $p<0.001$; ****, $p<0.0001$. All CHX-blocking assays were analyzed by one-way ANOVA.

# Figure 6

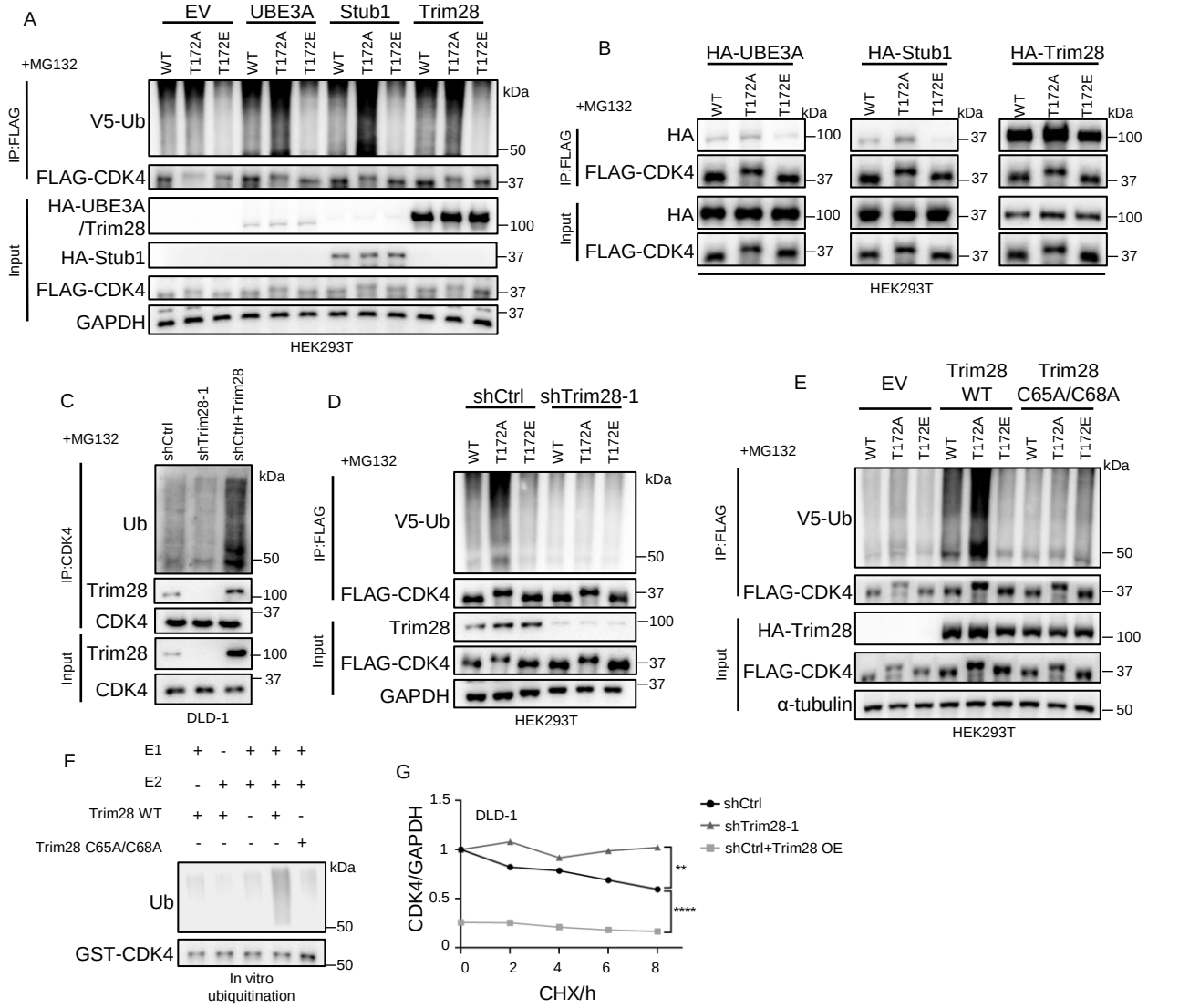
A
EV
UBE3A
Stub1
Trim28
WT
T172A
T172E
+MG132
IP:FLAG
V5-Ub
FLAG-CDK4
Input
HA-UBE3A /Trim28
HA-Stub1
FLAG-CDK4
GAPDH
kDa
HEK293T
B
HA-UBE3A
HA-Stub1
HA-Trim28
HA
FLAG-CDK4
C
shCtrl
shTrim28-1
shCtrl+Trim28
IP:CDK4
Ub
Trim28
CDK4
DLD-1
D
shCtrl
shTrim28-1
E
EV
Trim28 WT
Trim28 C65A/C68A
HA-Trim28
α-tubulin
F
E1
E2
Trim28 WT
Trim28 C65A/C68A
GST-CDK4
In vitro ubiquitination
G
DLD-1
CDK4/GAPDH
CHX/h
shCtrl
shTrim28-1
shCtrl+Trim28 OE
**
****

**Figure 6. Trim28 ubiquitinates CDK4 for protein degradation in the absence of T172 phosphorylation.** (**A**) Ubiquitination assay showing Trim28, UBE3A and Stub1 ubiquitinated CDK4 WT and T172A instead of T172E. MG132 was pretreated to maintain the same protein level. (**B**) Co-IP assay of CDK4 and CDK4 mutants with UBE3A, Stub1 and Trim28 showing the stronger binding of T172A and weaker binding of T172E with the E3 ligases. MG132 was pretreated to maintain the same protein level. (**C**) Ubiquitination assay of endogenous CDK4 under Trim28 knockdown and overexpression conditions. Trim28 was positively correlated with the ubiquitination of CDK4. MG132 was added to maintain the same protein level. (**D**) Ubiquitination assay showing the ubiquitination of CDK4 (WT and mutants) diminished under Trim28 knockdown condition. MG132 was pretreated to maintain the same protein level. (**E**) Ubiquitination assay showing the ubiquitination of CDK4 by Trim28 required the enzymatic activity of Trim28. C65A/C68A: Trim28 enzymatic dead mutant. MG132 was pretreated to maintain the same protein level. (**F**) In vitro ubiquitination assay showing Trim28 required ligase activity to ubiquitinate CDK4. (**G**) Statistic analysis of CHX-blocking assay showing endogenous CDK4 stability was negatively correlated with Trim28. By one-way ANOVA. **, $p<0.01$; ****, $p<0.0001$.

# Figure 7

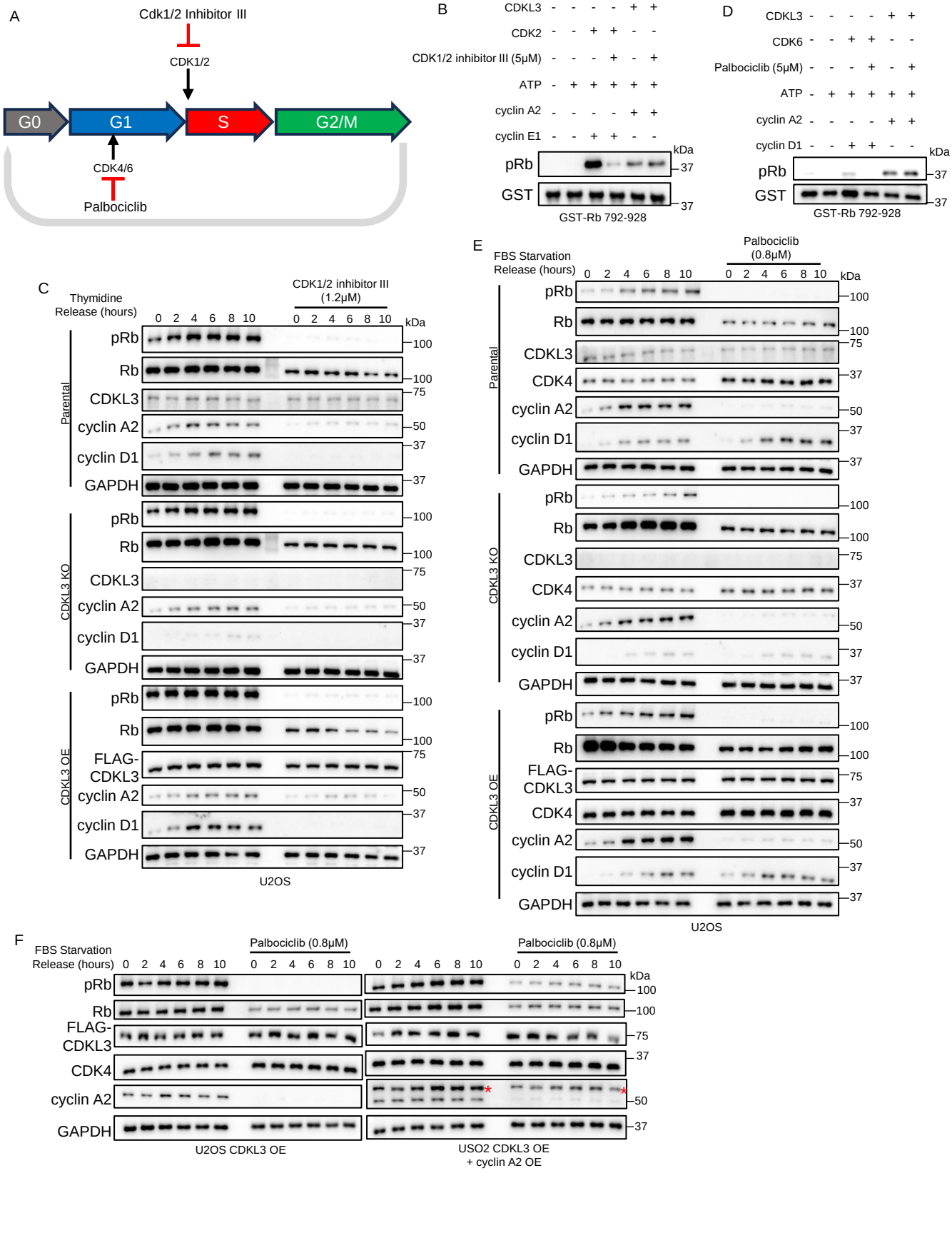
A
Cdk1/2 Inhibitor III
CDK1/2
G0
G1
S
G2/M
CDK4/6
Palbociclib
B
CDKL3
CDK2
CDK1/2 inhibitor III (5μM)
ATP
cyclin A2
cyclin E1
pRb
GST
kDa
37
GST-Rb 792-928
D
CDKL3
CDK6
Palbociclib (5μM)
ATP
cyclin A2
cyclin D1
pRb
GST
kDa
37
GST-Rb 792-928
C
Thymidine
Release (hours)
0 2 4 6 8 10
CDK1/2 inhibitor III
(1.2μM)
0 2 4 6 8 10
kDa
Parental
CDKL3 KO
CDKL3 OE
pRb
Rb
CDKL3
FLAG-
CDKL3
cyclin A2
cyclin D1
GAPDH
100
75
50
37
U2OS
E
FBS Starvation
Release (hours)
0 2 4 6 8 10
Palbociclib
(0.8μM)
0 2 4 6 8 10
kDa
Parental
CDKL3 KO
CDKL3 OE
pRb
Rb
CDKL3
FLAG-
CDKL3
CDK4
cyclin A2
cyclin D1
GAPDH
100
75
50
37
U2OS
F
FBS Starvation
Release (hours)
0 2 4 6 8 10
Palbociclib (0.8μM)
0 2 4 6 8 10
Palbociclib (0.8μM)
0 2 4 6 8 10
0 2 4 6 8 10
kDa
pRb
Rb
FLAG-
CDKL3
CDK4
cyclin A2
GAPDH
100
75
50
37
*
U2OS CDKL3 OE
USO2 CDKL3 OE
+ cyclin A2 OE

**Figure 7. CDK inhibitors do not affect CDKL3 kinase activity.** (**A**) Schematic drawing of the cell cycle inhibition by CDK4/6 inhibitor and CDK1/2 inhibitor. CDK1/2 inhibitor III: Cdk1/2 inhibitor; Palbociclib: CDK4/6 inhibitor. (**B**) In vitro kinase assay showing CDK2 inhibitor had no effect on the kinase activity of CDKL3 when phosphorylating Rb. (**C**) Immunoblotting of multiple cell cycle related proteins with double thymidine blocking and release and CDK1/2 inhibitor III treatment (1.2μM) under parental, CDKL3 knockout or overexpression conditions in U2OS cells. CDKL3 cannot affect G1-to-S transition. (**D**) In vitro kinase assay showing CDK4/6 inhibitor had no effect on the kinase activity of CDKL3 when phosphorylating Rb. (**E**) Immunoblotting of multiple cell cycle related proteins after serum starvation and release and Palbociclib treatment (0.8μM) under parental, CDKL3 knockout or overexpression conditions in U2OS cells. CDKL3 cannot compensate the inhibition of CDK4/6. (**F**) Immunoblotting assay showing CDKL3 can partially maintain Rb phosphorylation and G1 progression upon overexpression of cyclin A2, but cannot fully compensate the function of CDK4/6 after serum starvation and release in U2OS cells. Red asterisks represent the overexpressed Myc-tagged cyclin A2.

# Figure 8

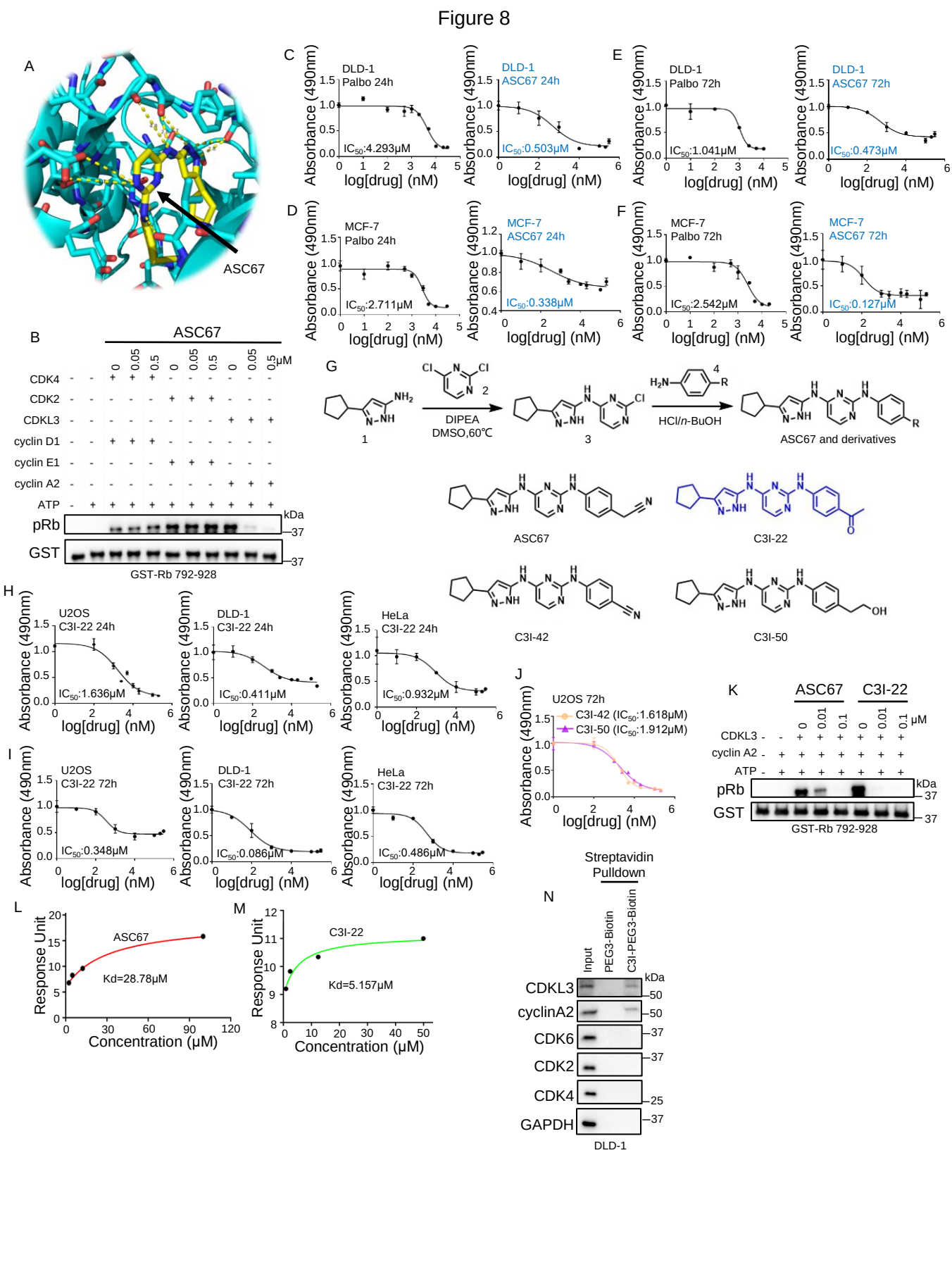
A
ASC67
B
ASC67
0
0.05
0.5
0
0.05
0.5
0
0.05
0.5 μM
CDK4
CDK2
CDKL3
cyclin D1
cyclin E1
cyclin A2
ATP
pRb
GST
kDa
37
37
GST-Rb 792-928
C
DLD-1
Palbo 24h
IC50:4.293μM
DLD-1
ASC67 24h
IC50:0.503μM
D
MCF-7
Palbo 24h
IC50:2.711μM
MCF-7
ASC67 24h
IC50:0.338μM
E
DLD-1
Palbo 72h
IC50:1.041μM
DLD-1
ASC67 72h
IC50:0.473μM
F
MCF-7
Palbo 72h
IC50:2.542μM
MCF-7
ASC67 72h
IC50:0.127μM
Absorbance (490nm)
log[drug] (nM)
G
1
DIPEA
DMSO,60℃
3
HCl/n-BuOH
ASC67 and derivatives
ASC67
C3I-22
C3I-42
C3I-50
H
U2OS
C3I-22 24h
IC50:1.636μM
DLD-1
C3I-22 24h
IC50:0.411μM
HeLa
C3I-22 24h
IC50:0.932μM
I
U2OS
C3I-22 72h
IC50:0.348μM
DLD-1
C3I-22 72h
IC50:0.086μM
HeLa
C3I-22 72h
IC50:0.486μM
J
U2OS 72h
C3I-42 (IC50:1.618μM)
C3I-50 (IC50:1.912μM)
K
ASC67
C3I-22
0
0.01
0.1
0
0.01
0.1 μM
CDKL3
cyclin A2
ATP
pRb
GST
kDa
37
37
GST-Rb 792-928
L
ASC67
Kd=28.78μM
Response Unit
Concentration (μM)
M
C3I-22
Kd=5.157μM
Response Unit
Concentration (μM)
N
Streptavidin Pulldown
Input
PEG3-Biotin
C3I-PEG3-Biotin
kDa
CDKL3
cyclinA2
CDK6
CDK2
CDK4
GAPDH
50
50
37
37
25
37
DLD-1

**Figure 8. Design and characterization of CDKL3 inhibitor.** (**A**) Structure of the kinase domain of CDKL3 with ASC67. Yellow dashes represent the potential hydrogen bonds between CDKL3 and ASC67. PDBID: 3ZDU. (**B**) In vitro kinase assay showing ASC67 specifically inhibited the kinase activity of CDKL3 to phosphorylate Rb dose-dependently. (**C-F**) Tumor-suppressing effects of Palbociclib and ASC67 treatments under different conditions. MCF-7 is an estrogen-responsive breast cancer cell line which is used as a direct comparison. (**G**) The synthesis route and chemical structures of ASC67, C3I-22, C3I-42, and C3I-50. The ASC67 and derivatives were synthesized via two steps. The compounds 1 and 2 reacted at the presence of DIPEA to obtain the intermediate 3. Then, the intermediate 3 can be substituted by different aniline derivatives 4 to afford ASC67 and its derivatives. (**H-J**) Tumor-suppressing effects of C3I-22 in different cancer cells at 24h (**H**) and 72h (**I**) and other derivatives at 72h (**J**). (**K**) In vitro kinase assay showing C3I-22 has stronger CDKL3-inhibitory function than ASC67. (**L, M**) Dissociation constants of CDKL3/ASC67 (**L**) and CDKL3/C3I-22 (**M**) binding acquired from Surface Plasmon Resonance (SPR). (**N**) Cellular pull-down assay showing C3I inhibitor has great selectivity in cells. All $IC_{50}$ analysis was triplicated.

**Table 1. List of $IC_{50}$ values of C3I-22 in different genetically-modified U2OS and DLD-1 cells.**

| Cell lines | $IC_{50}$ (μM), 24h | $IC_{50}$ (μM), 72h |
|---|---|---|
| U2OS | | |
| Parental | 1.317 | 0.415 |
| CDKL3 KO | Insensitive | Insensitive |
| CDKL3 OE | 6.93 | 7.826 |
| CDK4 KO | 0.484 | 0.23 |
| CDK4 OE | 6.855 | 3.735 |
| Rb KO | Insensitive | Insensitive |
| Rb OE | 0.678 | 0.165 |
| DLD-1 | | |
| Parental | 0.6 | 0.147 |
| CDKL3 KO | Insensitive | Insensitive |
| CDKL3 OE | 11.151 | 9.586 |
| CDK4 KO | 0.303 | 0.079 |
| CDK4 OE | 7.315 | 4.931 |
| Rb KO | Insensitive | Insensitive |
| Rb OE | 0.108 | 0.051 |

# Figure 9

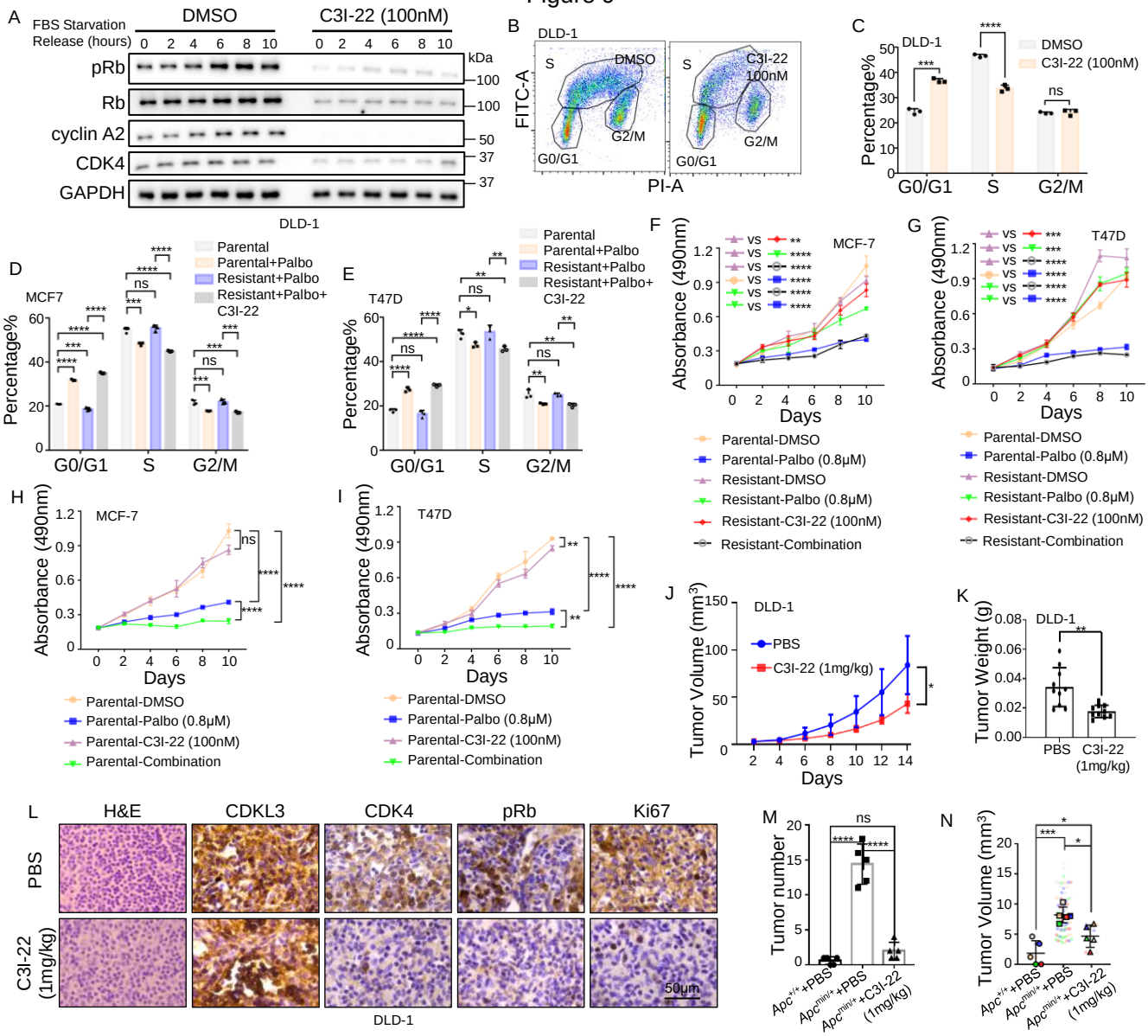
A
FBS Starvation
Release (hours)
DMSO
C3I-22 (100nM)
0 2 4 6 8 10
0 2 4 6 8 10
kDa
pRb
Rb
cyclin A2
CDK4
GAPDH
100
100
50
37
37
DLD-1
B
DLD-1
S
DMSO
G2/M
G0/G1
C3I-22
100nM
FITC-A
PI-A
C
DLD-1
DMSO
C3I-22 (100nM)
Percentage%
G0/G1
S
G2/M
ns
D
MCF7
Parental
Parental+Palbo
Resistant+Palbo
Resistant+Palbo+
C3I-22
Percentage%
G0/G1
S
G2/M
E
T47D
F
MCF-7
Absorbance (490nm)
Days
Parental-DMSO
Parental-Palbo (0.8μM)
Resistant-DMSO
Resistant-Palbo (0.8μM)
Resistant-C3I-22 (100nM)
Resistant-Combination
G
T47D
H
MCF-7
Parental-C3I-22 (100nM)
Parental-Combination
I
T47D
J
DLD-1
PBS
C3I-22 (1mg/kg)
Tumor Volume (mm3)
K
DLD-1
Tumor Weight (g)
L
H&E
CDKL3
CDK4
pRb
Ki67
PBS
C3I-22 (1mg/kg)
50μm
DLD-1
M
Tumor number
Apc+/+ +PBS
Apcmin/+ +PBS
Apcmin/+ +C3I-22 (1mg/kg)
N
Tumor Volume (mm3)

**Figure 9. C3I-22 (HZ1) antagonizes cancer growth via cell cycle arrest in multiple models.** (**A**) Immunoblotting assay showing C3I-22 treatment (100nM) reduced the levels of pRb and CDK4 after serum starvation and release in DLD-1 cells. (**B, C**) Flow cytometry results of BrdU/PI dual-staining showing C3I-22 treatment (100nM) caused cell cycle arrest in DLD-1 cells. (**B**), the representative result. (**C**), the statistical analysis. Error bar means ± SD, n=3, by two-tailed Student's t-test. (**D, E**) Flow cytometry of BrdU/PI dual-staining showing combinatorial treatment of Palbociclib and C3I-22 effectively caused cell cycle arrest at G0/G1 phase in the resistant MCF7 (**D**) and T47D (**E**) cells. Error bar means ± SD, n=3, by one-way ANOVA. (**F, G**) MTT assay showing C3I-22 treatment abolished the acquired resistance of Palbociclib in MCF7 (**F**) and T47D (**G**) cells. Error bars mean ± SD, n=3, two-way ANOVA. (**H, I**) MTT assay showing C3I-22 treatment sensitized MCF7 (**H**) and T47D (**I**) cells to Palbociclib. Error bars mean ± SD, n=3, two-way ANOVA. (**J, K**) Quantitative analyses of the tumor volume (**J**) and weight (**K**) of subcutaneously transplanted DLD-1 cells under different treatment. Tumor volume: Error bars mean ± SD, n=10, two-way ANOVA. Tumor weight: Error bar means ± SD, n=10, two-tailed Student's t-test. (**L**) Representative IHC staining and hematoxylin-eosin staining images of subcutaneously transplanted DLD-1 cells under different treatment. (**M, N**) Tumor number (**M**) and volume (**N**) in the intestines of *Apc*$^{min/+}$ mice under different treatments. **M**, error bar means ± SD, n=5, by one-way ANOVA. **N**, error bar means ± SD, 5 mice per group, by one-way ANOVA, *Apc*$^{+/+}$+PBS, n=3; *Apc*$^{min/+}$+PBS, n=71; *Apc*$^{min/+}$+C3I-22, n=10. Palbo: Palbociclib. All images in the same panel are under the same amplification scales. ns, not significant; *, p<0.05; **, p<0.01; ***, p<0.001; ****, p<0.0001.

**Table 2. List of $IC_{50}$ values of Palbociclib in parental or resistant hormone-sensitive breast cancer cell lines (MCF7 and T47D).**

| Cell lines | $IC_{50}$ (μM), 24h | $IC_{50}$ (μM), 72h |
|---|---|---|
| MCF7 | | |
| Parental | 2.878 | 2.57 |
| Resistant | 12.44 | 10.54 |
| Resistant+C3I-22 | 1.535 | 1.341 |
| T47D | | |
| Parental | 2.147 | 1.857 |
| Resistant | 11.832 | 12.019 |
| Resistant+C3I-22 | 1.732 | 1.038 |

C3I-22 was administrated at 100nM.

# Figure 10

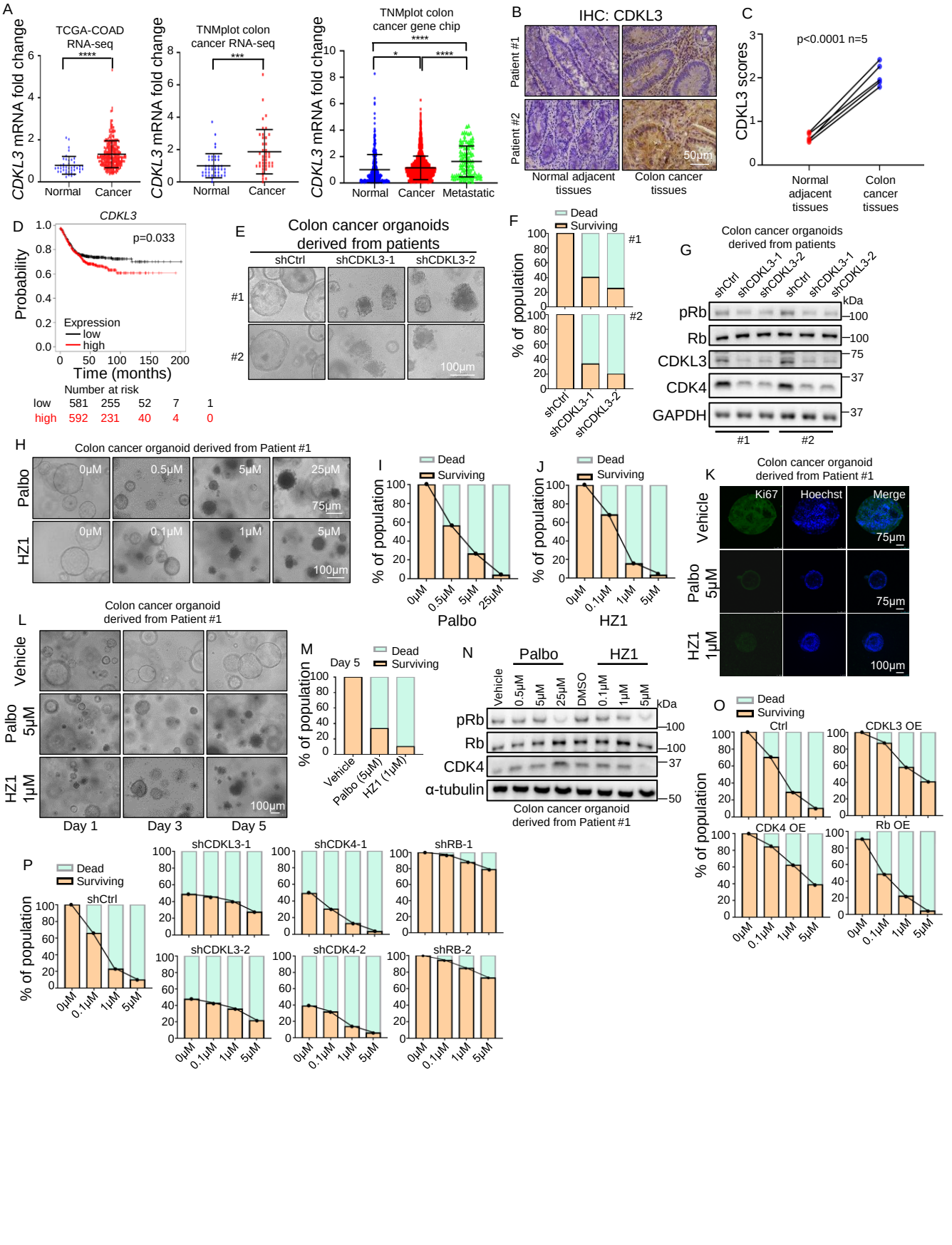
A
TCGA-COAD RNA-seq
TNMplot colon cancer RNA-seq
TNMplot colon cancer gene chip
CDKL3 mRNA fold change
Normal
Cancer
Metastatic
B
IHC: CDKL3
Patient #1
Patient #2
Normal adjacent tissues
Colon cancer tissues
50μm
C
CDKL3 scores
p<0.0001 n=5
D
CDKL3
p=0.033
Probability
Expression
low
high
Time (months)
Number at risk
low 581 255 52 7 1
high 592 231 40 4 0
E
Colon cancer organoids derived from patients
shCtrl
shCDKL3-1
shCDKL3-2
100μm
F
Dead
Surviving
% of population
G
pRb
Rb
CDKL3
CDK4
GAPDH
kDa
H
Colon cancer organoid derived from Patient #1
Palbo
HZ1
0μM
0.5μM
5μM
25μM
0.1μM
1μM
75μm
100μm
I
Palbo
J
HZ1
K
Ki67
Hoechst
Merge
Vehicle
L
Day 1
Day 3
Day 5
M
Day 5
Vehicle
Palbo (5μM)
HZ1 (1μM)
N
α-tubulin
DMSO
O
Ctrl
CDKL3 OE
CDK4 OE
Rb OE
P
shCtrl
shCDKL3-1
shCDKL3-2
shCDK4-1
shCDK4-2
shRB-1
shRB-2

**Figure 10. HZ1 has strong clinical implication in colon cancer treatment.** (**A**) Multiple transcriptome databases showing *CDKL3* had higher expression in colon cancer than the normal tissues. Error bar means ± SD, by two-tailed Student's t-test (if 2 sets of data) or one-way ANOVA (if 3 sets of data). (**B**) Representative IHC staining images showing the higher CDKL3 protein level in colon cancer tissues. (**C**) CDKL3 immunohistochemical score in colon cancerous and normal adjacent tissues. Error bar means ± SD, n=5, two-tailed Student's t-test. (**D**) Correlation analysis between *CDKL3* expression and poor prognosis in patients with colon cancer, by Kaplan Meyer-plotter. (**E, F**) Representative images (**E**) and quantification (**F**) of patient-derived colon cancer organoids (PDCCO) after CDKL3 depletion. (**G**) Immunoblotting assay showing CDKL3 depletion reduced the levels of pRb and CDK4 in PDCCO. (**H**) Representative images of PDCCO under treatments. (**I, J**) Quantification of the surviving/dead organoids percentage under Palbociclib (**I**) and HZ1 (**J**) treatments in **H**. (**K**) Representative immunofluorescence images of PDCCO under Palbociclib and HZ1 treatment. Ki67: proliferation marker. (**L**) Representative images of PDCCO under Palbociclib and HZ1 treatment at different time points and different dosages. (**M**) Quantification of the surviving/dead organoids percentage under treatments at Day 5. (**N**) Immunoblotting assay showing HZ1 decreased the levels of pRb and CDK4 in patient-derived colon cancer organoids. (**O, P**) Quantification of the surviving/dead organoids percentage under CDKL3/CDK4/Rb overexpression (**O**) or depletion (**P**) conditions. Palbo: Palbociclib. All images in the same panel are under the same amplification scales unless specified. *, $p<0.05$; ***, $p<0.001$; ****, $p<0.0001$.